Modelling plant species distribution in alpine grasslands using airborne imaging spectroscopy

Julien Pottier, Zbynek Malenovsky, Achilleas Psomas, Lucie Homolova, Michael E. Schaepman, Philippe Choler, Wilfried Thuiller, Antoine Guisan, Niklaus E Zimmermann

1-1-2014

Modelling plant species distribution in alpine grasslands using airborne imaging spectroscopy

Julien Pottier
University of Lausanne

Zbynek Malenovký
University of Wollongong, zbynek@uow.edu.au

Achilleas Psomas
Swiss Federal Research Institute WSL

Lucie Homolova
University of Zurich

Michael E. Schaepman
University of Zurich

See next page for additional authors

Modelling plant species distribution in alpine grasslands using airborne imaging spectroscopy

Abstract

Remote sensing using airborne imaging spectroscopy (AIS) is known to retrieve fundamental optical properties of ecosystems. However, the value of these properties for predicting plant species distribution remains unclear. Here, we assess whether such data can add value to topographic variables for predicting plant distributions in French and Swiss alpine grasslands. We fitted statistical models with high spectral and spatial resolution reflectance data and tested four optical indices sensitive to leaf chlorophyll content, leaf water content and leaf area index. We found moderate added-value of AIS data for predicting alpine plant species distribution. Contrary to expectations, differences between species distribution models (SDMs) were not linked to their local abundance or phylogenetic/functional similarity. Moreover, spectral signatures of species were found to be partly site-specific. We discuss current limits of AIS-based SDMs, highlighting issues of scale and informational content of AIS data.

Keywords

species distribution, reflectance, hyperspectral data, alpine grasslands

Publication Details

Pottier, J., Malenovsky, Z., Psomas, A., Homolova, L., Schaepman, M. E., Choler, P., Thuiller, W., Guisan, A. & Zimmermann, N. E. (2014). Modelling plant species distribution in alpine grasslands using airborne imaging spectroscopy. Biology Letters, 10 (7), 1-4.

Authors

Julien Pottier, Zbynek Malenovký, Achilleas Psomas, Lucie Homolova, Michael E. Schaepman, Philippe Choler, Wilfried Thuiller, Antoine Guisan, and Niklaus E. Zimmermann

Title:

MODELLING PLANT SPECIES DISTRIBUTION IN ALPINE GRASSLANDS USING AIRBORNE IMAGING SPECTROSCOPY.

Authors:

Julien Pottier[1,2], Zbyněk Malenovský[3,4], Achilleas Psomas[5], Lucie Homolová[3], Michael E. Schaepman[3], Philippe Choler[6,7,8], Wilfried Thuiller[6,7*], Antoine Guisan[1*], and Niklaus E. Zimmermann[5*]

Authors' affiliation:

[1]Department of Ecology and Evolution, Biophore 1015, Lausanne, Switzerland

[2]INRA, UR874, F-63100, Clermont-Ferrand, France

[3]Remote Sensing Laboratories, University of Zürich, 8057 Zürich, Switzerland

[4]School of Biological Sciences, University of Wollongong, Northfields Ave, NSW 2522, Australia

[5]Swiss Federal Research Institute WSL, 8903 Birmensdorf, Switzerland

[6]Univ. Grenoble Alpes, LECA, F-38000 Grenoble, France

[7]CNRS, LECA, F-38000 Grenoble, France

[8]Station Alpine Joseph Fourier, UMS CNRS-UJF 3370, Univ. Grenoble Alpes F-38041, Grenoble Cedex 9, France

[*] shared last authorship

Number of figures: 2

Electronic supplementary material:

ESM1: Details on data acquisition, processing and modelling.

ESM2: Complementary results.

Abstract:

Remote sensing using airborne imaging spectroscopy (AIS) is known to retrieve fundamental optical properties of ecosystems. However, the value of these properties for predicting plant species distribution remains unclear. Here, we assess whether such data can add value to topographic variables for predicting plant distributions in French and Swiss alpine grasslands. We fitted statistical models with high spectral and spatial resolution reflectance data and tested four optical indices sensitive to leaf chlorophyll content, leaf water content and leaf area index. We found moderate added-value of AIS-data for predicting alpine plant species distribution. Contrary to expectations, differences between species distribution models were not linked to their local abundance or phylogenetic/functional similarity. Moreover, spectral signatures of species were found to be partly site-specific. We discuss current limits of AIS-based species distribution models, highlighting issues of scale and informational content of AIS-data.

Keywords:

species distribution, reflectance, hyperspectral data, alpine grasslands.

1. INTRODUCTION

Spatial modelling of species distributions is commonly used to forecast environmental change effects, detect biodiversity hotspots or predict species' invasions [1]. As fine-grained environmental descriptors are difficult to obtain, coarse-grained (from hundred of metres to kilometres) topo-climatic descriptors are usually used. Recent advances in airborne imaging spectroscopy (AIS) have allowed the acquisition of images with high spectral and sub-metre spatial resolution [2]. Spectral information provided by remotely-sensed reflectance is influenced by phenology, variations in morphological, structural and biochemical properties

of species [3], as well as by local environmental conditions (e.g. hydric stress, soil properties or productivity [4,5]) that determine species habitat suitability [6]. Nevertheless, previous attempts to predict species distributions with hyperspectral data have generated mixed results [7,8]. Sub-metre resolution allows the targeting of small plants and micro-habitats where species find refuge, highlighting potential benefits of hyperspatial remote sensing for biodiversity monitoring [9]. However, despite increased spatial and spectral resolution of airborne data, little is known about its value in modelling species' distributions in species-rich ecosystems characterised by fine-scale heterogeneity.

Here, we explore the predictive power of AIS-data for modelling plant species distributions in alpine grasslands in two distinct regions. Specifically, we aim to: i) identify key remotely-sensed spectral information for predicting the distribution of grassland species; and ii) assess whether AIS-data substantially improves model predictions. We also test for any phylogenetic or functional dependency of model characteristics among species.

2. MATERIAL AND METHODS

(a) Study sites and species data

The study was conducted in the Western French (FR) and Western Swiss (CH) Alps (Electronic Supplementary Material (ESM) 1). The French site included 103 vegetation plots of 2-5m in radius, located between 2000 and 2830 metres above sea level (m.a.s.l.). The Swiss site included 68 quadrats (2 by 2 m) located between 1650 and 2150 m.a.s.l. Species cover was visually estimated using the Braun-Blanquet abundance scale. In total 160 species were selected for species distribution analysis (119 species in FR, 78 in CH). Thirty-seven species were common to both sites (see ESM 1 for the details on selection criteria).

(b) Remote sensing data

AIS-data were acquired with the dual Airborne Imaging Spectroradiometer for Applications (AISA; Specim Ltd., Finland). Raw AISA images contained 359 spectral bands between 400 and 2450 nm with spectral resolution ranging from 4.3 to 6.3 nm, and a pixel size of 0.8 m. After image processing, we extracted two types of AIS-predictors: i) reflectance in 75 spectral bands (avoiding bands with noisy radiometric response), and ii) four vegetation indices. Vegetation indices characterized leaf chlorophyll (TCARI/OSAVI and ANCB) [10], leaf water content (SIWSI) [11] and leaf area index (MTVI2) [12] (for details see ESM 1). Removal of poorly-vegetated plots resulted in datasets with 70 FR and 53 CH plots.

(c) Topographic predictors

We computed five predictors derived from digital elevation models at 50 m resolution for FR and 25 m resolution for CH, representing meso-scale habitat conditions : i) elevation (metre), ii) slope (degree), iii) aspect (degree), iv) topographic position index (unitless), and v) topographic wetness index (unitless) (see ESM 1).

(d) Species distribution modelling

Species distribution models (SDMs) were fitted with five different sets of variables: i) topographic predictors only, ii) reflectance predictors only, iii) vegetation indices only, iv) topographic and reflectance predictors combined, and v) topographic predictors and vegetation indices combined. We first used a conditional Random Forest algorithm to estimate the unbiased relative importance of predictors in the case of multi-colinearity, then ran final models based on selection of the most important predictors [13] (see ESM 1). Their predictive accuracy was evaluated within each study site separately using a repeated split-sample procedure (100 iterations). 70% of the sample points were used for model calibration and 30% for model evaluation in each iteration.

(e) Model differences among species

105 The relative importance of AIS-predictors and the predictive accuracy of SDMs were tested against 1)
106 species' phylogenetic relatedness, 2) species' functional similarity, including a set of morphological
107 and physiological traits that are well correlated with the reflectance of canopy stands [14] (see ESM 2,
108 section 5), and 3) species' abundance patterns within plots. Phylogenetic and functional tests were
109 computed as described in [15] (see ESM 2, section 5).
110
111 ## 3. RESULTS
112 When fitting SDMs with reflectance data the analysis of predictor importance indicated
113 similarities in the selected spectral bands among sites (Figure 1). The most important spectral
114 bands were located between 500 and 900 nm for both sites, but site-specific differences in
115 important spectral bands were also apparent (1500-1800 nm in FR, 1200-1500 nm and 2000-
116 2500 nm in CH). These site differences existed for species present at only one or both sites
117 (ESM 2, Figure 1). On average, all vegetation indices showed similar importance for SDM
118 fitting (ESM 2, Figure 2).
119 The prediction accuracy of SDMs based solely on topographic predictors, reflectance data or
120 vegetation indices did not differ significantly. However, SDMs including both AIS and
121 topographic predictors tended to be more accurate (Figure 2 and ESM 2, Table 1). The
122 improvement was marginally significant for vegetation indices (Wilcoxon rank sum test, p
123 =0.079) but non-significant for reflectance in FR. Conversely, CH showed significant
124 improvement when using reflectance (Wilcoxon rank sum test, $p = 0.012$), but non-significant
125 effects when using vegetation indices. Improvements when including AIS-predictors differed
126 among species, with few species showing ≥10% improved predictions and many showing
127 reduced predictive accuracy (ESM 2, Figure 3). These variations were independent of species'
128 abundance patterns and species' phylogenetic or functional similarity (ESM 2, Figures 4-13).
129
130 ## 4. DISCUSSION

Overall, topographic and AIS-based SDMs revealed similar predictive accuracies in both sites. Model accuracy was on average higher in FR than in CH, while the topographical and spectral ranges observed in CH were much narrower than in FR (ESM 1, Figures 2, 4, 5). This agrees with previous studies where accuracy of SDMs derived from satellite images increased with steepness of ecological gradients [6]. Unlike vegetation indices, we found that importance of spectral bands differed between sites. Site-specific differences may partly reflect canopy differences due to nutrient status or soil chemistry since reflectance in these spectral regions is sensitive to light absorption by water [12], biochemical constituents [14] and scattering by plant architecture [11]. Additional field measurements of vegetation properties could probably improve ecological understanding of these spectral regions in SDMs.

The distribution models fit differed between species. Overall, models including both topographic and AIS-predictors tended to be more accurate, even though significant improvements were confined to a limited number of species. This contrasts with results reported for invasive weeds [16], but agrees with results from meadows [7] where plant assemblages are inextricably mixed at the fine scale. Benefits of high spatial resolution of remote-sensing data is a subject of debate [17]. Although our methodology considers the existence of geometric misalignment between AIS-images and plot georeferencing, it still represents a source of uncertainty for matching reflectance of small pixels with local species occurrence. The significance of this uncertainty for species distribution modelling remains to be assessed.

We expected that differences between species models in terms of predictive accuracy and relative importance of AIS-predictors would be linked to i) abundance of species within-plots since locally-dominant species contribute more to canopy reflectance, and ii) phylogenetic or functional similarity, assuming that similar species show either comparable spectral signatures

or similar habitat requirements as reflected by AIS-data. These hypotheses were not supported. We suggest two possible explanations for such idiosyncrasy. Firstly, accurate estimation of species' similarity may be limited by uncertainties in phylogenetic trait conservatism or availability of plant functional trait data. Phylogenies can often contribute to the integrated comparison of plant functional and life-history traits among species. However, the evolution of traits is characterized by both conservatism and diversification, and close links between functional similarity and phylogenetic relatedness are not always found [18]. In the present study, we described species' functional similarity using morphological and ecophysiological traits that are recognized as key canopy reflectance drivers [14]. However, biochemical traits such as leaf nitrogen, chlorophyll or phosphorus content were not available for all species, and should be included wherever possible. Secondly, AIS-based SDMs may reflect both species' spectral signature and micro-habitat suitability [19] (contrary to topography-based models which reflect solely habitat suitability at meso-scales). These two factors may differ in importance when fitting AIS-variables across species and sites. This would explain why AIS-based models of both locally-dominant (species detection scenario, e.g. *Dryas octopetalla*), and low-abundance species (habitat suitability scenario, e.g. *Helictotrichon sedense*) show equivalent accuracy despite very different species contributions to canopy characteristics and functional traits. Future research should focus on discriminating between species detection and habitat suitability for an array of species and ecosystem types (of varying degree of vegetation complexity), to better assess the ecological relevance of imaging spectroscopy for species' distribution modelling.

Data accessibility:

Data available from the Dryad Digital Repository：doi:10.5061/dryad.n13hn

Acknowledgements

This study was initiated and funded by the European ECOCHANGE project (GOCE-CT-2007-036866) and the Swiss National Science Foundation (BIOASSEMBLE, 31003A-125145). WT received funding from the ERC (EC FP7, 281422 (TEEMBIO)), MS from UZH URPP 'Global Change and Biodiversity'. Computations were performed at the HPC Vital-IT Centre (Swiss Institute of Bioinformatics). Logistic support was provided by the 'Station Alpine Joseph Fourier' in France. We are grateful to all persons supporting data collection. We also thank J.M.G. Bloor and four anonymous referees for helpful comments on previous version of the manuscript.

References

1. Guisan, A. & Thuiller, W. 2005 Predicting species distribution: offering more than simple habitat models. *Ecol. Lett.* **8**, 993–1009. (doi:10.1111/j.1461-0248.2005.00792.x)

2. Schaepman, M. E., Ustin, S. L., Plaza, A. J., Painter, T. H., Verrelst, J. & Liang, S. 2009 Earth system science related imaging spectroscopy—An assessment. *Remote Sens. Environ.* **113**, S123–S137. (doi:10.1016/j.rse.2009.03.001)

3. Ustin, S. L. & Gamon, J. A. 2010 Remote sensing of plant functional types. *New Phytol.* **186**, 795–816. (doi:10.1111/j.1469-8137.2010.03284.x)

4. Schmidtlein, S. 2005 Imaging spectroscopy as a tool for mapping Ellenberg indicator values. *J. Appl. Ecol.* **42**, 966–974. (doi:10.1111/j.1365-2664.2005.01064.x)

5. Parviainen, M., Luoto, M. & Heikkinen, R. K. 2010 NDVI-based productivity and heterogeneity as indicators of plant-species richness in boreal landscapes. *Boreal Environ. Res.* **15**, 301–318.

6. Feilhauer, H., He, K. S. & Rocchini, D. 2012 Modeling species distribution using niche-based proxies derived from composite bioclimatic variables and MODIS NDVI. *Remote Sens.* **4**, 2057–2075. (doi:10.3390/rs4072057)

7. Schmidtlein, S. & Sassin, J. 2004 Mapping of continuous floristic gradients in grasslands using hyperspectral imagery. *Remote Sens. Environ.* **92**, 126–138. (doi:doi: 10.1016/j.rse.2004.05.004)

8. Lawrence, R. L., Wood, S. D. & Sheley, R. L. 2006 Mapping invasive plants using hyperspectral imagery and Breiman Cutler classifications (randomForest). *Remote Sens. Environ.* **100**, 356–362. (doi:10.1016/j.rse.2005.10.014)

9. Rocchini, D. 2007 Effects of spatial and spectral resolution in estimating ecosystem α-diversity by satellite imagery. *Remote Sens. Environ.* **111**, 423–434. (doi:10.1016/j.rse.2007.03.018)

10. Malenovský, Z., Homolová, L., Zurita-Milla, R., Lukeš, P., Kaplan, V., Hanuš, J., Gastellu-Etchegorry, J.-P. & Schaepman, M. E. 2013 Retrieval of spruce leaf chlorophyll content from airborne image data using continuum removal and radiative transfer. *Remote Sens. Environ.* **131**, 85–102. (doi:10.1016/j.rse.2012.12.015)

11. Haboudane, D., Millera, J. R., Pattey, E., Zarco-Tejada, P. J. & Strachan, I. B. 2004 Hyperspectral vegetation indices and novel algorithms for predicting green LAI of crop canopies: Modeling and validation in the context of precision agriculture. *Remote Sens. Environ.* **90**, 337–352. (doi:10.1016/j.rse.2003.12.013)

12. Cheng, Y.-B., Zarco-Tejada, P. J., Riaño, D., Rueda, C. A. & Ustin, S. L. 2006 Estimating vegetation water content with hyperspectral data for different canopy scenarios: Relationships between AVIRIS and MODIS indexes. *Remote Sens. Environ.* **105**, 354–366. (doi:10.1016/j.rse.2006.07.005)

13. Strobl, C., Boulesteix, A.-L., Kneib, T., Augustin, T. & Zeileis, A. 2008 Conditional variable importance for random forests. *BMC Bioinformatics* **9**, 307. (doi:10.1186/1471-2105-9-307)

14. Homolová, L., Malenovský, Z., Clevers, J. G. P. W., García-Santos, G. & Schaepman, M. E. 2013 Review of optical-based remote sensing for plant trait mapping. *Ecol. Complex.* **15**, 1–16. (doi:10.1016/j.ecocom.2013.06.003)

15. Hardy, O. J. & Pavoine, S. 2012 Assessing phylogenetic signal with measurement error: a comparison of Mantel tests, Blomberg et al.'s K, and phylogenetic distograms. *Evolution* **66**, 2614–21. (doi:10.1111/j.1558-5646.2012.01623.x)

16. Lawrence, R. L., Wood, S. D. & Sheley, R. L. 2006 Mapping invasive plants using hyperspectral imagery and Breiman Cutler classifications (RandomForest). *Remote Sens. Environ.* **100**, 356–362. (doi:10.1016/j.rse.2005.10.014)

17. Nagendra, H. & Rocchini, D. 2008 High resolution satellite imagery for tropical biodiversity studies: the devil is in the detail. *Biodivers. Conserv.* **17**, 3431–3442. (doi:10.1007/s10531-008-9479-0)

18. Ackerly, D. D. 2009 Conservatism and diversification of plant functional traits: Evolutionary rates versus phylogenetic signal. *Proc. Natl. Acad. Sci. U. S. A.* **106 Suppl** , 19699–706. (doi:10.1073/pnas.0901635106)

19. Bradley, B. a., Olsson, A. D., Wang, O., Dickson, B. G., Pelech, L., Sesnie, S. E. & Zachmann, L. J. 2012 Species detection vs. habitat suitability: Are we biasing habitat

suitability models with remotely sensed data? *Ecol. Modell.* **244**, 57–64. (doi:10.1016/j.ecolmodel.2012.06.019)

253 **Figure 1:** Relative importance of reflectance intensity in spectral bands for predicting species
254 distributions at study sites in France (FR) and Switzerland (CH). Variable importance was
255 assessed using conditional inference in Random Forest models. Gray areas represent bands
256 used for the calculation of vegetation indices.
257
258 **Figure 2:** Prediction accuracy of species distribution models (based on the area under the
259 curve of a receiver-operating characteristic plot: AUC) built with Random Forest models at
260 study sites in France (FR) and Switzerland (CH). Topo indicates topographic-predictors, BS
261 indicates reflectance recorded in the spectral bands and VI indicates vegetation indices.
262

Figure 1

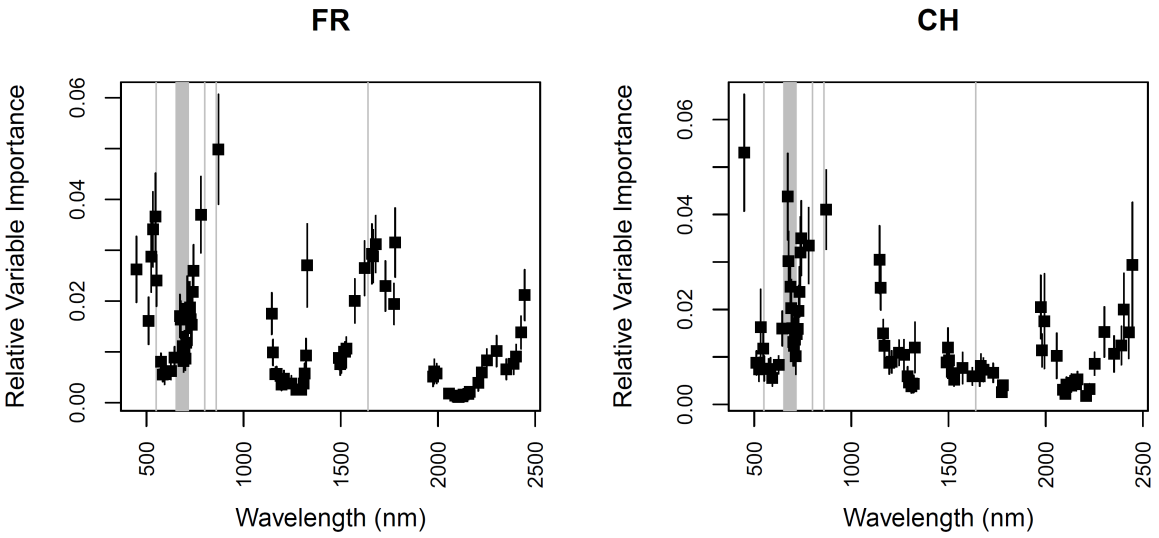

Figure 2

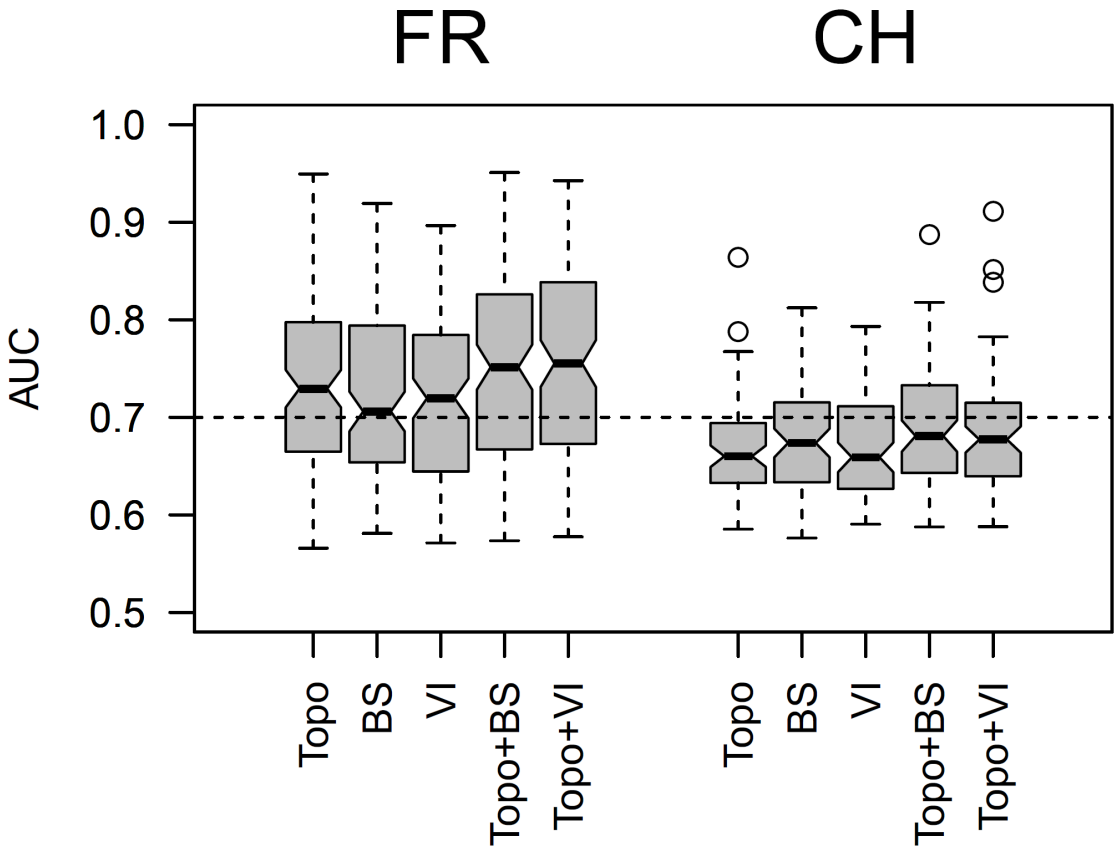

Electronic Supplementary Material 1:

Details on data acquisition, processing and modelling.

1) The study sites

ESM 1 Table 1: Topographic, environmental and floristic characteristics of the two study areas.

	French site (FR)	Swiss site (CH)
Location name	Roche Noire	Anzeindaz
Geographic coordinates	45°2.3' to 45°4.2'N 6°21.6' to 6°25.2'E	46°15' to 46°18'N, 7°07' to 7°11'E
Elevation range	1900 m to 3000 m	1650 m to 2150 m
Mean annual temperature	4.8°C	1.3 °C
Mean summer precipitation	180 mm	485 mm
Bed rock	Flysch	Calcareous
Number of inventoried plots	103	68

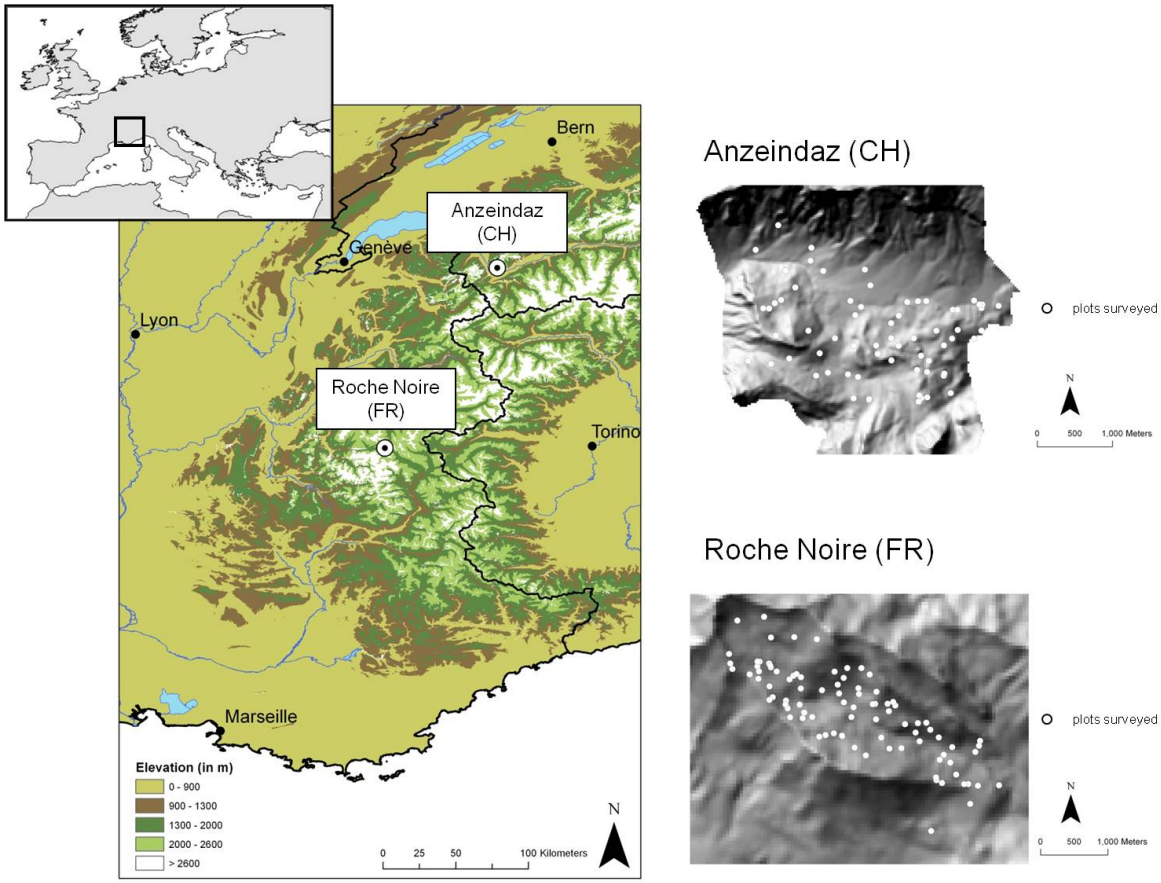

ESM 1 Fig. 1: Location of the two study areas. The minimum distance between vegetation plots is 21.91 m (mean of 1327.71 m) for FR and 12.67 m (mean of 1307.44 m) for CH.

2) Floristic data

Vegetation sampling was based on random stratified sampling designs to ensure covering equally well the different vegetation types of both FR and CH. Size of vegetation plots was chosen to approach exhaustive recording of the species. As vegetation structure differed between both sites, 2 m quadrat was chosen for CH and plots of 5 m in radius for FR. In addition, few plots of 2 m in radius were chosen in FR for sampling snowbelts. In such habitats species coexist at very fine scale so that reduced plot size still allow exhaustive sampling of the species of local vegetation patches. However, snowbelts are also characterised by fine scale vegetation changes in space. Thus, plots of 2 m in radius, compare to 5 m in radius, avoided bias in sampling associated vegetation type by edge effects.

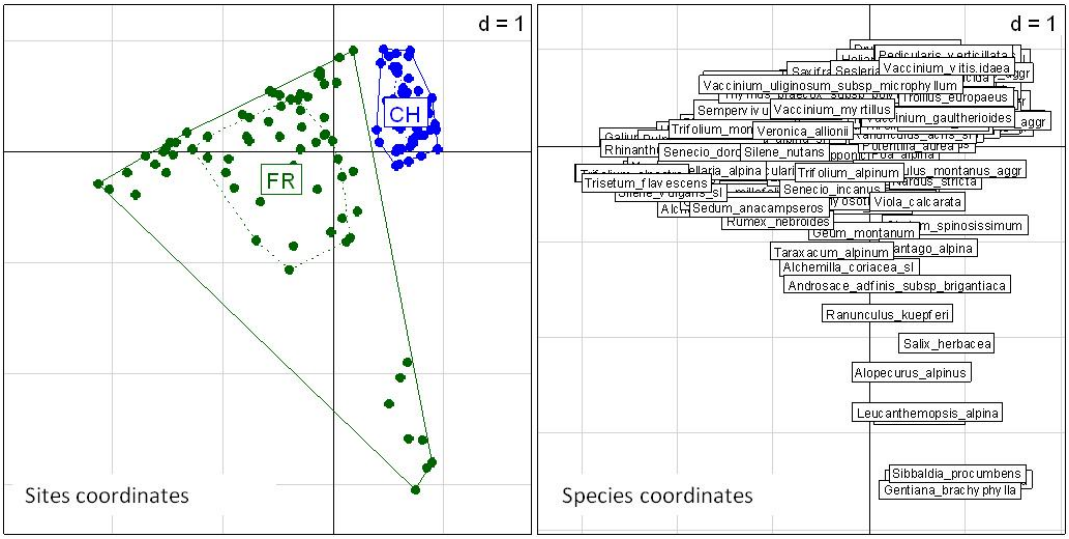

ESM1 Fig 2: Correspondence analysis of floristic data. Between site inertia ratio = 0.06 with *Pvalue*<0.001(Permutation test with 9999 permutations, alternative is greater).

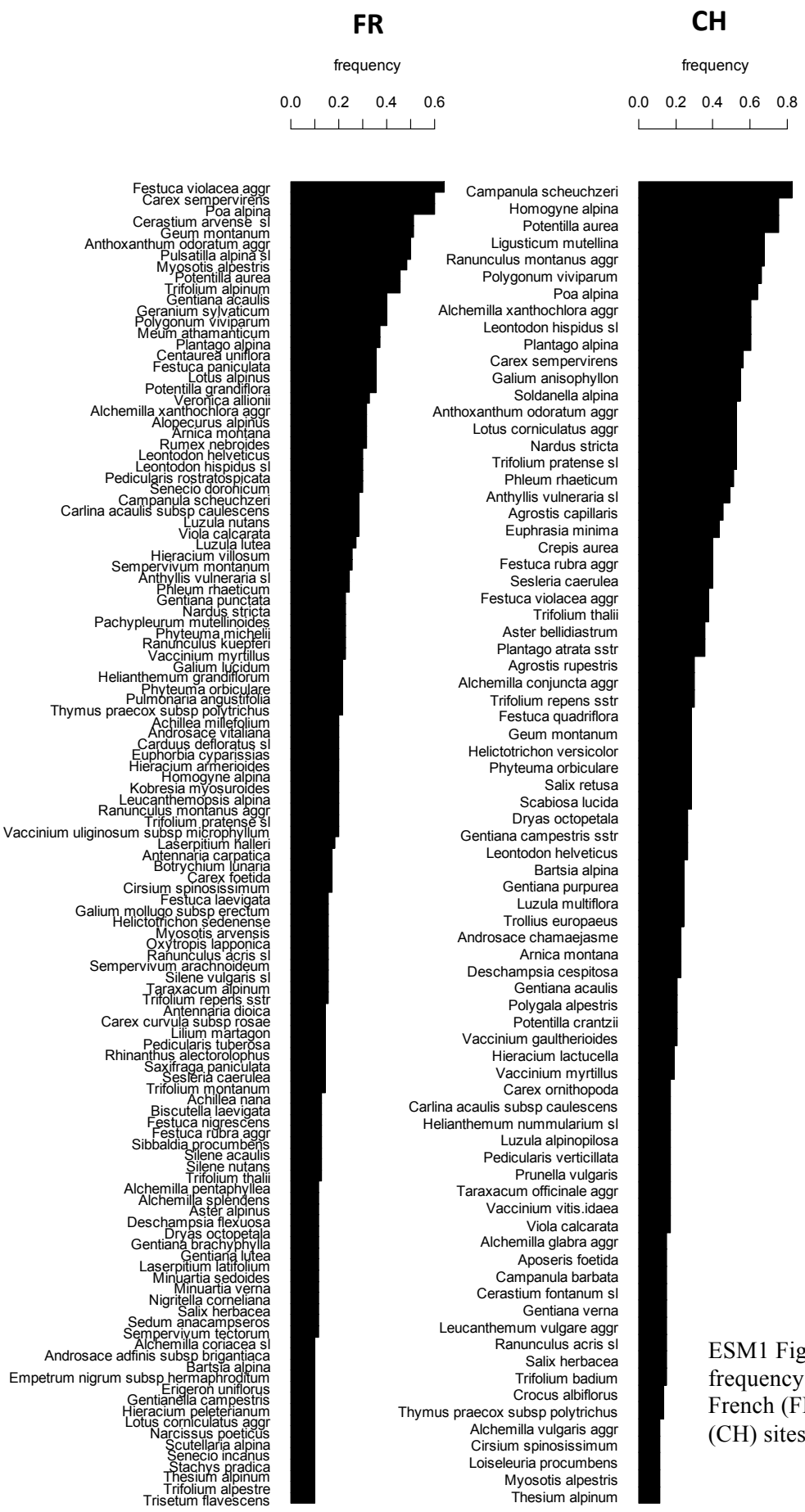

ESM1 Fig 3: Species rank-frequency curves for the French (FR) and Swiss (CH) sites.

3) Topographic predictors

We computed five predictors derived from digital elevation models at 50 m resolution for FR and 25 m resolution for CH, providing useful information on meso-scale habitat conditions in species distribution models [1]. Topographic predictors were: 1) elevation (in meters); 2) slope (in degrees); 3) aspect (in degrees from north); 4) Topographic Position Index (TPI), an integrated measure of topographic exposure (unitless) [2]; 5) Topographic Wetness Index (TWI), which quantifies topographic control on soil moisture (unitless), [3]. The last is calculated as follows TWI = ln(a / tan(b)) where a is the area of the upstream contribution (flow accumulation) and b is the slope in radians .

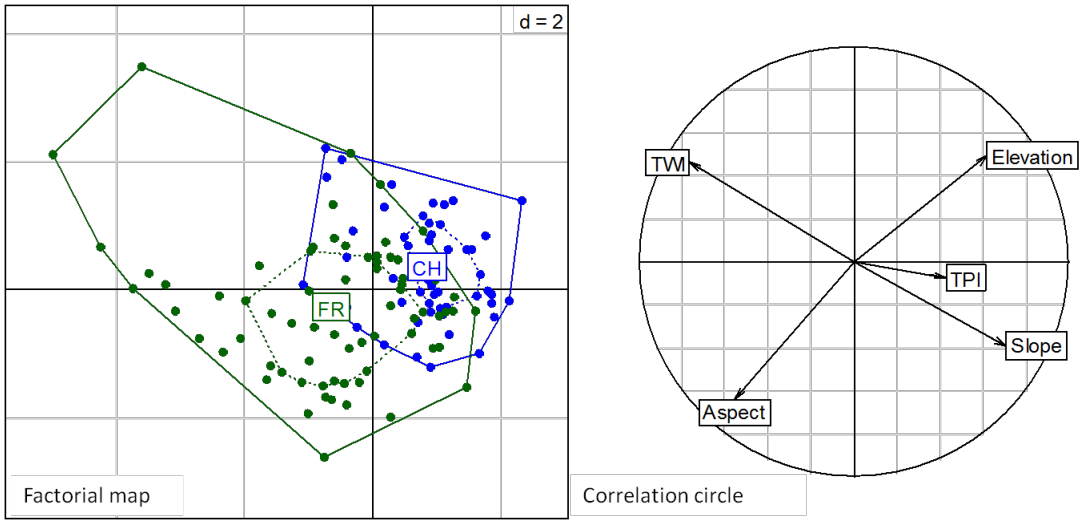

ESM1 Fig 4: Principal component analysis of the topographic predictors. Between site inertia ratio = 0.14 with *Pvalue*<0.001(Permutation test with 9999 permutations, alternative is greater). This result shows that topographical conditions of vegetation plots differ between the French (FR) and Swiss (CH) sites.

4) Remote sensing predictors

a. Airborne image acquisition and processing

The airborne imaging spectroscopy (AIS) data were acquired with an AISA Dual system (Specim, Ltd. Finland). Images of the French study site (FR) were collected on 23rd July 2008

and for the Swiss study site (CH) on 24th July 2008 under clear sky and sunny conditions. Images were acquired in a high spectral and spatial resolution mode, which resulted in a spectral image data cube with 359 narrow spectral bands between 400 and 2450 nm and the ground pixel size of 0.8 m.

The basic processing of AISA Dual images comprised of radiometric, geometric, and atmospheric correction. The radiometric correction that converted image digital numbers into radiance values [$W.m^{-2}.sr^{-1}.\mu m^{-1}$] was performed in the CaliGeo software (CaliGeo v.4.6.4 - AISA processing toolbox, Specim, 2007) using the factory delivered radiometric calibration coefficients. Images were geometrically corrected using the onboard navigation data from the Inertial Navigation System and a local digital elevation model (spatial resolution of 2.5 m for FR and 1 m for CH site). Images were further orthorectified into the Universal Transverse Mercator (UTM, Zone 32N) map projection. An accuracy of the geometric correction was evaluated by calculating an average root mean square error (RMSE) between distinct image displayed and ground measured control points. Assessment resulted into an average RMSE of about 2.04 m for the French site and about 1.25 m for the Swiss site. Atmospheric corrections were combined with vicarious radiometric calibrations in the ATCOR-4 software [4]. To eliminate random noise, spectra of the atmospherically corrected images were smoothed by a moving average filter with the window size of 7 bands. Accuracy of the atmospheric corrections was evaluated by comparing image surface reflectance with a set of ground measured reference spectra. An average reflectance RMSE between the image and the ground target spectra was equal to 2.1% for the French and 1.6% for the Swiss site. As the final step of the image processing we applied a fully constrained linear spectral unmixing algorithm [5] to identify pixels with high vegetation fraction. Only pixels with vegetation fraction higher than 75% were included into further analysis of species distribution modelling.

We paired the AISA image data with the georeferenced plots, where floristic species composition was investigated in-situ. Their geographical locations were superimposed over the AISA images and the reflectance function of each a research plot was averaged. Plots with high proportion of non-vegetated pixels (i.e. pixels with vegetation fraction lower than 75% due to the occurrence of stones or bare soil patches) were excluded. After this selection, we retained 70 plots at the French site and 53 plots at the Swiss site. Two types of remote sensing predictors were tested for the species distribution modelling: i) reflectance intensity of 75 noise-free bands and ii) four vegetation indices (summarized in Table 2).

b. Removal of spectral bands with low signal quality

Only 75 spectral bands out of 359 were included in the species distribution analysis. We removed bands with poor signal quality due to the low radiometric sensitivity at the edges of both sensor spectral ranges (401-444, 876-1140 and around 2450 nm), bands strongly influenced by atmospheric water vapor absorption (i.e., 1334-1485 and 1786-1968 nm) and adjacent bands of near infrared wavelengths between 752 and 771 nm, which are highly correlated and contain redundant spectral information.

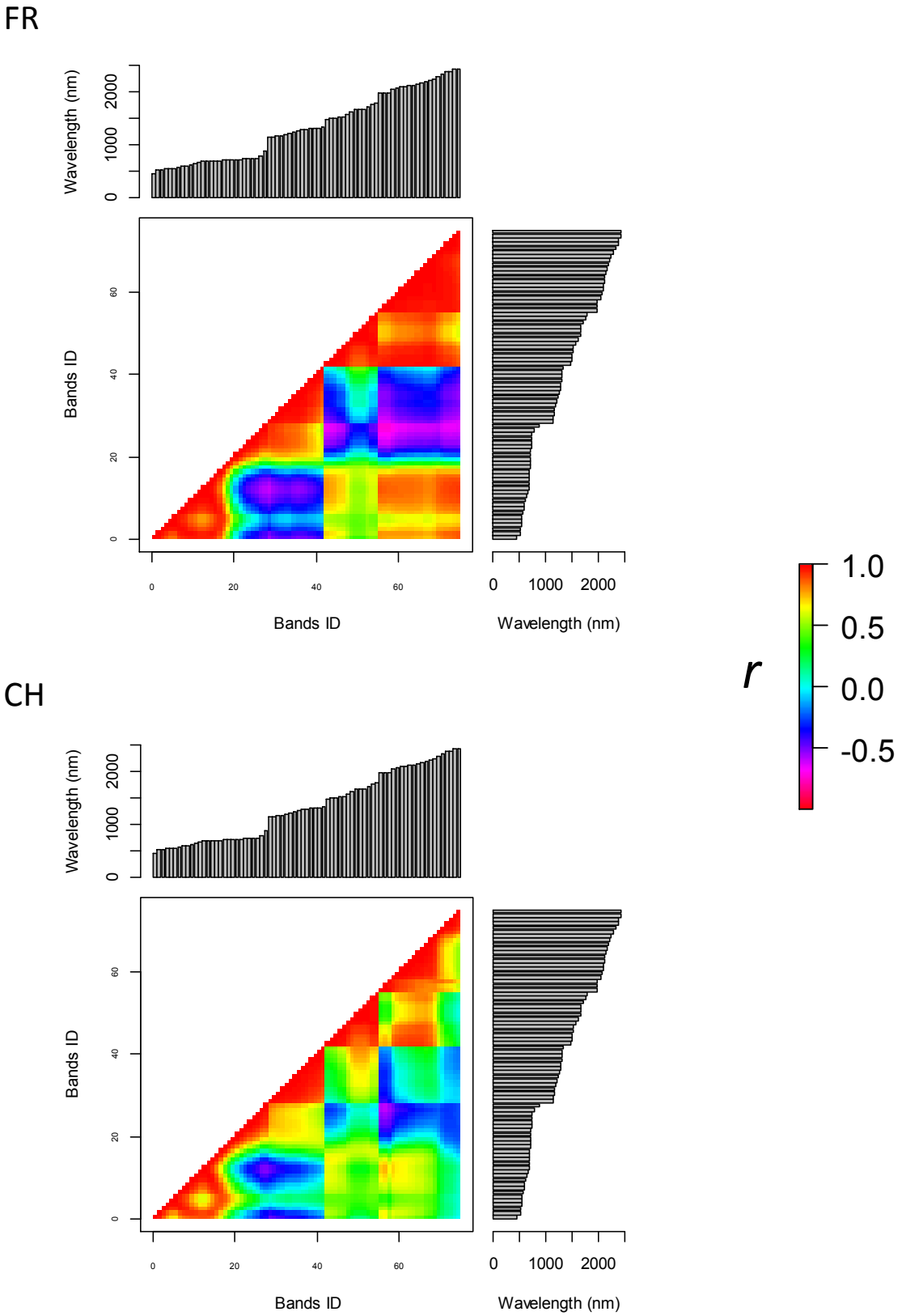

373

374

ESM1 Fig 5: Between reflectance bands correlation patterns for the French (FR) and Swiss (CH) sites. Although band selection (75 out of 359) led to the removal of highly correlated adjacent bands, many non-adjacent bands were strongly correlated. This justifies the use of unbiased conditional random forest in case of multicolinearity.

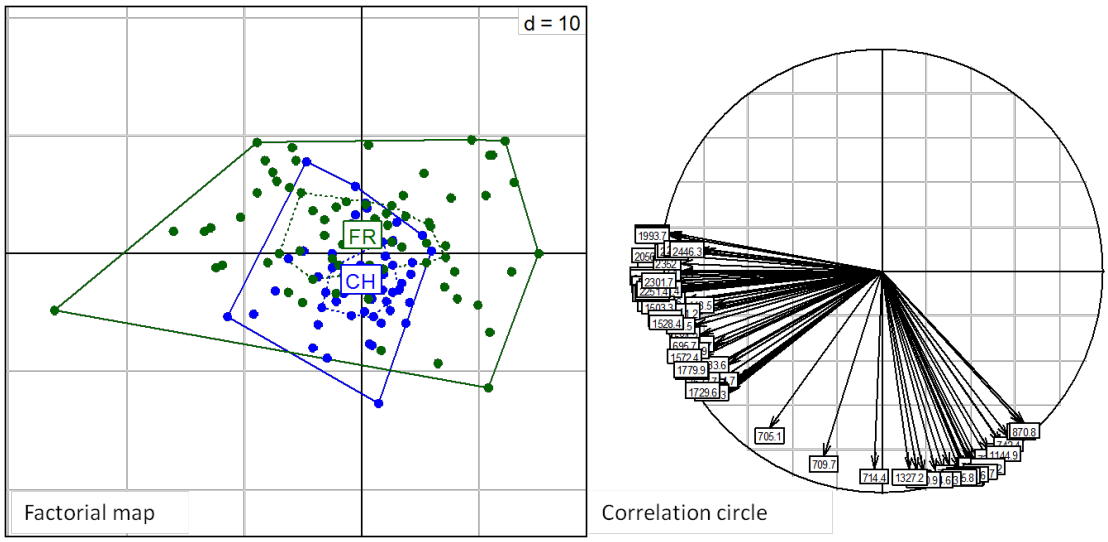

ESM1 Fig 6: Principal component analysis of the 75 reflectance bands. Between site inertia ratio = 0.06 with *Pvalue*<0.001(Permutation test with 9999 permutations, alternative is greater). This result shows that reflectance pattern of vegetation plots differed between the French (FR) and Swiss (CH) sites.

c. Calculation of vegetation indices and the between site PCA

Four vegetation optical indices, defined in Table 2, were selected as remote sensing indicators of the vegetation biochemical and biophysical properties. Two indices are highly sensitive to leaf chlorophyll content, but insensitive to the variations in amount of green biomass (TCARI/OSAVI and $ANCB_{650\text{-}720}$). MTVI2 index was chosen as an indicator of green leaf area index, while suppressing negative confounding influence of leaf chlorophyll content. Finally, SIWSI index is sensitive to plant water content. The variability of the selected optical indices is expected to be species composition specific in accordance with the species-specific changes of the related biochemical and biophysical characteristics. These four indices can thus potentially discriminate key properties of the species, justifying their use for species distribution modeling.

EMS 1 Table 2: Vegetation indices tested for species distribution modeling

Vegetation index	Equation		Reference
Transformed Chlorophyll Absorbtion Reflectance Index / Optimized Soil-Adjusted Vegetation Index (TCARI/OSAVI)	$\mathrm{TCARI} = 3[\mathrm{R}_{700} - \mathrm{R}_{670} - 0.2(\mathrm{R}_{700} - \mathrm{R}_{550})(\mathrm{R}_{700}/\mathrm{R}_{670})]$ $\mathrm{OSAVI} = \frac{1.16(R_{800} - R_{670})}{R_{700} + R_{670} + 0.16}$		Haboudane et al, (2002) [5]
Area under curve Normalized to the Continuum-removed Band depth ($ANCB_{650\text{-}720}$)	$\frac{\mathrm{AUC}_{650-720}}{\mathrm{CBD}_{670}}$	where $AUC_{650\text{-}720}$ is area under continuum removed reflectance between 650-720 nm and CBD_{670} is continuum removed band depth at 670 nm	Malenovský et al. (2013) [6]
Modified Triangular Vegetation Index (MTVI2)	$\frac{1.5[1.2(\mathrm{R}_{800} - \mathrm{R}_{550}) - 2.5(\mathrm{R}_{670} - \mathrm{R}_{550})]}{\sqrt{(2\mathrm{R}_{800} + 1)^2 - (6\mathrm{R}_{800} - 5\sqrt{\mathrm{R}_{570}}) - 0.5}}$		Haboudane et al. (2004) [7]
Shortwave Infrared Water Stress Index (SIWSI)	$\frac{\mathrm{R}_{858.5} - \mathrm{R}_{1640}}{\mathrm{R}_{858.5} + \mathrm{R}_{1640}}$		Cheng et al. (2006) [8]

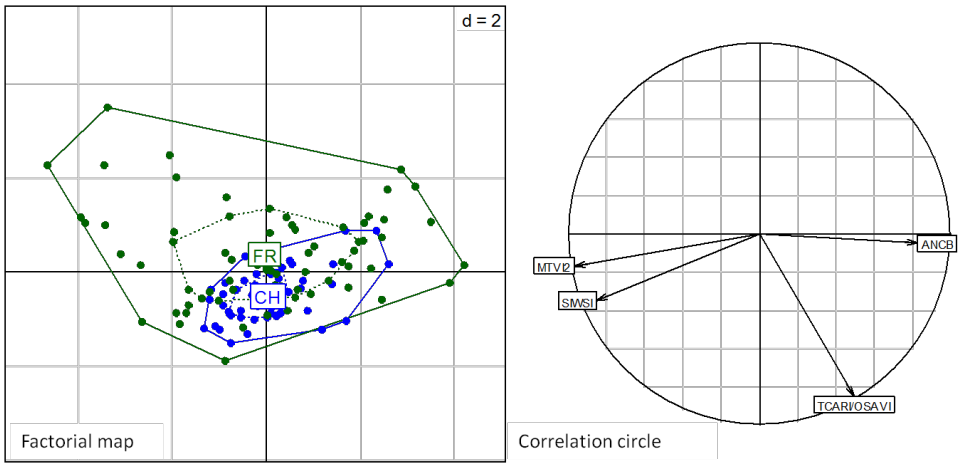

ESM1 Fig 7: Principal component analysis of the remote sensing predictors (vegetation indices. Between site inertia ratio = 0.05 with *Pvalue*=0.003 (Permutation test with 9999 permutations, alternative is greater). This result shows that reflectance indices of vegetation plots differed between the French (FR) and Swiss (CH) sites.

d. Correlation of AIS-data with topographic predictors

AIS and topographical data were weakly correlated (max absolute values for Pearson correlations amounted to 0.40-0.55 between elevation and bands in the range of 2000 and 2500 nm, while most of absolute values for Pearson correlation coefficients are between 0 and 0.3). Absence of strong correlation allows for mixing both types of data in species distribution models, as topographic- (indicating meso-scale habitat suitability of the species) and fine-scale AIS-data may represent complementary information.

5) Selection of spectral bands for building final species distribution models

Based on the analysis performed to quantify the importance of each of the 75 spectral bands, we built final species distribution models according to the following variable selection procedure:

1. Rank bands in decreasing order of importance
2. While not all bands have been considered, select the first ranked band (with the highest relative importance) and remove all bands showing correlation >0.7 with the previously selected band.

This procedure was performed with random forest (RF) using conditional inference trees as base learners and was implemented with the *party* library [9] for R [10]. Variable importance is measured as the mean decrease in accuracy of model predictions after permuting the predictor variables.

References

1. Pradervand, J.-N., Dubuis, A., Pellissier, L., Guisan, A. & Randin, C. 2013 Very high resolution environmental predictors in species distribution models: Moving beyond topography? *Prog. Phys. Geogr.* **38**, 79–96. (doi:10.1177/0309133313512667)

2. Zimmermann, N. E., Edwards, T. C., Moisen, G. G., Frescino, T. S. & Blackard, J. A. 2007 Remote sensing-based predictors improve distribution models of rare, early successional and broadleaf tree species in Utah. *J. Appl. Ecol.* **44**, 1057–1067. (doi:10.1111/j.1365-2664.2007.01348.x)

3. Beven, K. J. & Kirkby, M. J. 1979 A physically based, variable contributing area model of basin hydrology. *Bull. Int. Assoc. Sci. Hydrol.* **24**, 43–69.

4. Richter, R. & Schlapfer, D. 2002 Geo-atmospheric processing of airborne imaging spectrometry data. Part 2: Atmospheric/topographic correction. *Int. J. Remote Sens.* **23**, 2631–2649. (doi:10.1080/01431160110115834)

5. Haboudane, D., Miller, J. R., Tremblay, N., Zarco-Tejada, P. J. & Dextraze, L. 2002 Integrated narrow-band vegetation indices for prediction of crop chlorophyll content for application to precision agriculture. *Remote Sens. Environ.* **81**, 416–426. (doi:10.1016/S0034-4257(02)00018-4)

6. Malenovský, Z., Homolová, L., Zurita-Milla, R., Lukeš, P., Kaplan, V., Hanuš, J., Gastellu-Etchegorry, J.-P. & Schaepman, M. E. 2013 Retrieval of spruce leaf chlorophyll content from airborne image data using continuum removal and radiative transfer. *Remote Sens. Environ.* **131**, 85–102. (doi:10.1016/j.rse.2012.12.015)

7. Haboudane, D., Millera, J. R., Pattey, E., Zarco-Tejada, P. J. & Strachan, I. B. 2004 Hyperspectral vegetation indices and novel algorithms for predicting green LAI of crop canopies: Modeling and validation in the context of precision agriculture. *Remote Sens. Environ.* **90**, 337–352. (doi:10.1016/j.rse.2003.12.013)

8. Cheng, Y.-B., Zarco-Tejada, P. J., Riaño, D., Rueda, C. A. & Ustin, S. L. 2006 Estimating vegetation water content with hyperspectral data for different canopy scenarios: Relationships between AVIRIS and MODIS indexes. *Remote Sens. Environ.* **105**, 354–366. (doi:10.1016/j.rse.2006.07.005)

9. Strobl, C., Hothorn, T. & Zeileis, A. 2009 Party on! A New, Conditional Variable Importance Measure for Random Forests Available in the party Package. , 1–4.

10. R Core Team 2013 R: A Language and Environment for Statistical Computing.

Electronic Supplementary Material 2:

Complementary results.

1) **Relative importance of reflectance intensity in spectral bands for predicting the distribution of species recorded only in one of the two sites or recorded in both sites.**

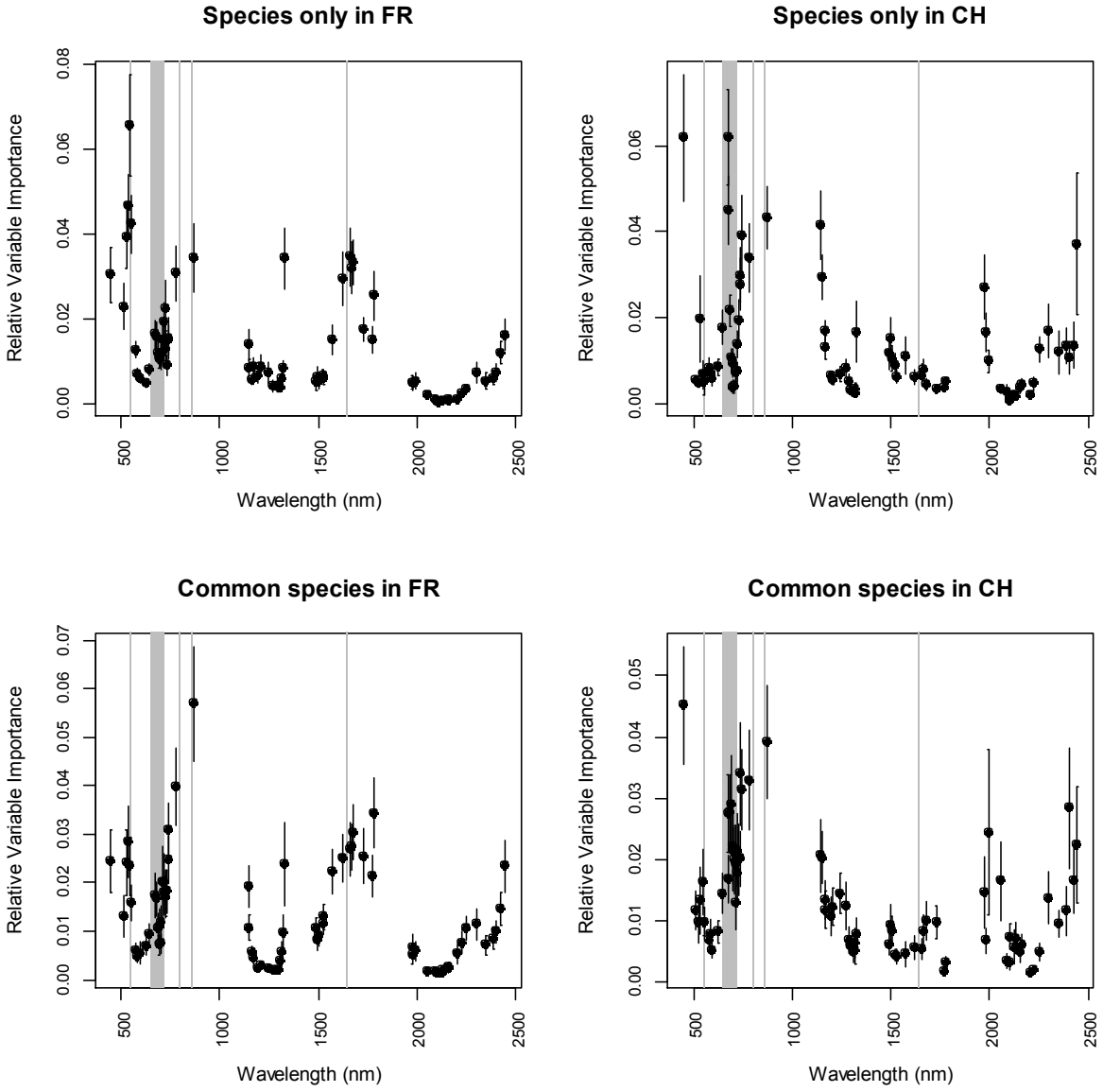

ESM2 Fig 1: Relative importance of reflectance intensity in spectral bands for predicting the distribution of species recorded only in the French site (FR), only in the Swiss site (CH), recorded in both sites but modeled in the French site and recorded in both sites but modeled in the Swiss site. Gray areas represent bands used for the calculation of the vegetation indices.

2) Variable importance of vegetation indices for the French site (FR) and the Swiss site (CH).

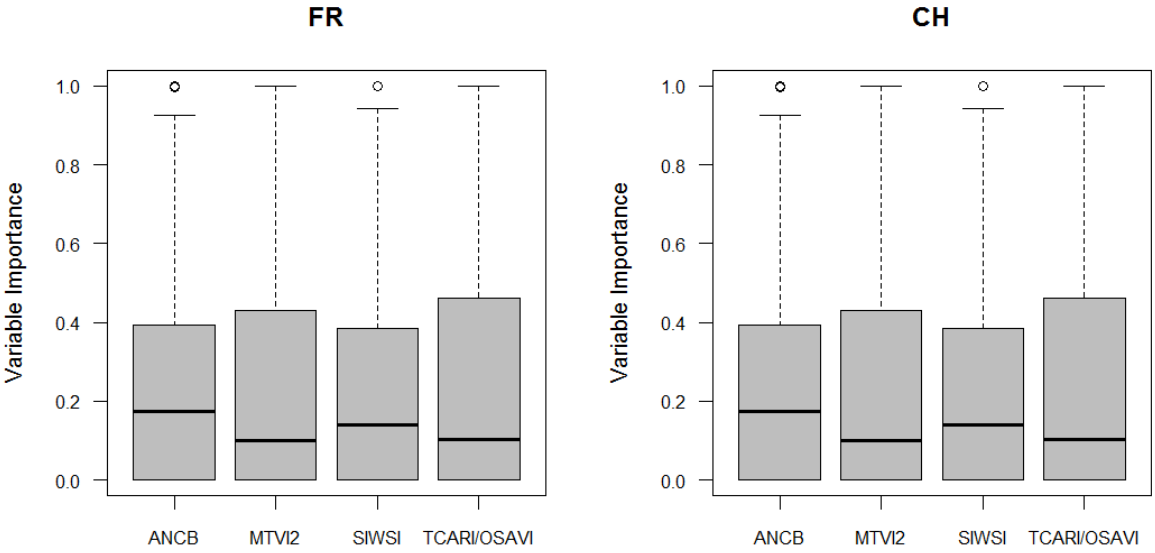

ESM2 Fig 2: Variable importance of the RS-retrieved vegetation indices for modeling species distribution. FR for the French site and CH for the Swiss site. Details on the calculation of indices can be found in ESM1.

3) Detailed prediction accuracy of species distribution models.

ESM 2 Table 1: Summary table of prediction accuracy of species distribution models assessed with the area under the curve of a receiver-operating characteristic plot: AUC. Topo indicates models based on topographic predictors only, BS models based on reflectance selected spectral bands. VI indicates models based on vegetation indices only. Topo+BS and Topo+VI indicate respectively models based on topographic predictors and reflectance or vegetation indices as predictors. Species are listed in alphabetic order according to their occurrence in the two sites. Green highlighting indicates species that showed at least 10% improvement of model accuracy when adding the AIS-predictors to topographic based models in at least one of the two sites. AUC values above 0.7 can be considered as models with good prediction accuracy.

	Topo		BS		Topo+BS		VI		Topo+VI	
	FR	CH	FR	CH	FR	CH	FR	CH	FR	CH
Achillea millefolium	0.686	-	0.807	-	0.811	-	0.8	-	0.827	-
Achillea nana	0.8	-	0.703	-	0.783	-	0.737	-	0.746	-
Alchemilla coriacea sl.	0.735	-	0.707	-	0.717	-	0.721	-	0.732	-
Alchemilla pentaphyllea	0.893	-	0.763	-	0.897	-	0.817	-	0.884	-
Alchemilla splendens	0.695	-	0.682	-	0.728	-	0.664	-	0.727	-
Alopecurus alpinus	0.742	-	0.607	-	0.704	-	0.668	-	0.733	-
Androsace adfinis subsp. *brigantiaca*	0.703	-	0.65	-	0.713	-	0.719	-	0.763	-

Androsace vitaliana	0.666	-	0.785	-	0.786	-	0.786	-	0.76	-
Antennaria carpatica	0.776	-	0.757	-	0.823	-	0.743	-	0.787	-
Antennaria dioica	0.783	-	0.675	-	0.783	-	0.639	-	0.737	-
Aster alpinus	0.703	-	0.689	-	0.664	-	0.662	-	0.711	-
Biscutella laevigata	0.795	-	0.631	-	0.722	-	0.627	-	0.755	-
Botrychium lunaria	0.681	-	0.704	-	0.679	-	0.722	-	0.711	-
Carduus defloratus sl.	0.852	-	0.796	-	0.817	-	0.751	-	0.836	-
Carex curvula subsp. *rosae*	0.789	-	0.803	-	0.827	-	0.82	-	0.764	-
Carex foetida	0.78	-	0.655	-	0.721	-	0.67	-	0.763	-
Centaurea uniflora	0.781	-	0.8	-	0.864	-	0.779	-	0.837	-
Cerastium arvense sl.	0.677	-	0.581	-	0.663	-	0.592	-	0.689	-
Deschampsia flexuosa	0.658	-	0.653	-	0.597	-	0.729	-	0.657	-
Empetrum nigrum subsp. *hermaphroditum*	0.943	-	0.843	-	0.933	-	0.897	-	0.931	-
Erigeron uniflorus	0.656	-	0.664	-	0.66	-	0.672	-	0.673	-
Euphorbia cyparissias	0.832	-	0.785	-	0.842	-	0.755	-	0.852	-
Festuca laevigata	0.846	-	0.681	-	0.859	-	0.702	-	0.87	-
Festuca nigrescens	0.607	-	0.705	-	0.658	-	0.686	-	0.62	-
Festuca paniculata	0.741	-	0.746	-	0.782	-	0.783	-	0.839	-
Galium lucidum	0.776	-	0.66	-	0.746	-	0.613	-	0.765	-
Galium mollugo subsp. *erectum*	0.87	-	0.756	-	0.848	-	0.73	-	0.874	-
Gentiana brachyphylla	0.882	-	0.664	-	0.859	-	0.736	-	0.903	-
Gentiana lutea	0.949	-	0.801	-	0.942	-	0.737	-	0.943	-
Gentiana punctata	0.709	-	0.706	-	0.708	-	0.692	-	0.71	-
Gentianella campestris	0.719	-	0.656	-	0.676	-	0.686	-	0.708	-
Geranium sylvaticum	0.775	-	0.796	-	0.801	-	0.82	-	0.821	-
Helianthemum grandiflorum	0.775	-	0.642	-	0.74	-	0.62	-	0.752	-
Helictotrichon sedenense	0.64	-	0.858	-	0.839	-	0.849	-	0.837	-
Hieracium armerioides	0.633	-	0.692	-	0.666	-	0.72	-	0.645	-
Hieracium peleterianum	0.645	-	0.692	-	0.635	-	0.673	-	0.648	-
Hieracium villosum	0.616	-	0.608	-	0.645	-	0.613	-	0.597	-
Kobresia myosuroides	0.68	-	0.695	-	0.732	-	0.738	-	0.73	-
Laserpitium halleri	0.73	-	0.803	-	0.771	-	0.718	-	0.701	-
Laserpitium latifolium	0.864	-	0.852	-	0.908	-	0.82	-	0.87	-
Leucanthemopsis alpina	0.734	-	0.822	-	0.861	-	0.829	-	0.858	-
Lilium martagon	0.819	-	0.806	-	0.789	-	0.783	-	0.839	-
Lotus alpinus	0.626	-	0.624	-	0.628	-	0.602	-	0.615	-
Luzula lutea	0.725	-	0.762	-	0.762	-	0.753	-	0.754	-
Luzula nutans	0.623	-	0.657	-	0.669	-	0.631	-	0.633	-
Meum athamanticum	0.829	-	0.919	-	0.931	-	0.881	-	0.888	-
Minuartia sedoides	0.783	-	0.77	-	0.806	-	0.779	-	0.767	-
Minuartia verna	0.753	-	0.824	-	0.817	-	0.821	-	0.896	-
Myosotis arvensis	0.85	-	0.859	-	0.876	-	0.822	-	0.847	-
Narcissus poeticus	0.935	-	0.875	-	0.951	-	0.886	-	0.942	-
Nigritella corneliana	0.615	-	0.592	-	0.622	-	0.631	-	0.621	-
Oxytropis lapponica	0.645	-	0.733	-	0.662	-	0.632	-	0.641	-

Pachypleurum mutellinoides	0.828	-	0.831	-	0.841	-	0.797	-	0.845	-
Pedicularis rostratospicata	0.64	-	0.592	-	0.647	-	0.624	-	0.642	-
Pedicularis tuberosa	0.748	-	0.758	-	0.786	-	0.686	-	0.765	-
Phyteuma michelii	0.75	-	0.686	-	0.752	-	0.66	-	0.727	-
Potentilla grandiflora	0.801	-	0.768	-	0.809	-	0.735	-	0.785	-
Pulmonaria angustifolia	0.781	-	0.781	-	0.801	-	0.779	-	0.837	-
Pulsatilla alpina sl.	0.566	-	0.601	-	0.574	-	0.594	-	0.584	-
Ranunculus kuepferi	0.727	-	0.612	-	0.693	-	0.6	-	0.698	-
Rhinanthus alectorolophus	0.864	-	0.869	-	0.932	-	0.847	-	0.926	-
Rumex nebroides	0.673	-	0.726	-	0.719	-	0.746	-	0.713	-
Saxifraga paniculata	0.665	-	0.843	-	0.853	-	0.861	-	0.846	-
Scutellaria alpina	0.864	-	0.777	-	0.894	-	0.777	-	0.879	-
Sedum anacampseros	0.691	-	0.643	-	0.676	-	0.705	-	0.693	-
Sempervivum arachnoideum	0.707	-	0.75	-	0.774	-	0.798	-	0.816	-
Sempervivum montanum	0.752	-	0.719	-	0.754	-	0.736	-	0.795	-
Sempervivum tectorum	0.745	-	0.645	-	0.756	-	0.623	-	0.776	-
Senecio doronicum	0.841	-	0.779	-	0.826	-	0.778	-	0.83	-
Senecio incanus	0.683	-	0.699	-	0.662	-	0.704	-	0.667	-
Sibbaldia procumbens	0.836	-	0.721	-	0.841	-	0.858	-	0.877	-
Silene acaulis	0.774	-	0.832	-	0.834	-	0.848	-	0.849	-
Silene nutans	0.683	-	0.678	-	0.669	-	0.642	-	0.633	-
Silene vulgaris sl.	0.736	-	0.813	-	0.777	-	0.711	-	0.761	-
Stachys pradica	0.764	-	0.669	-	0.743	-	0.672	-	0.74	-
Taraxacum alpinum	0.64	-	0.631	-	0.613	-	0.644	-	0.661	-
Trifolium alpestre	0.874	-	0.88	-	0.916	-	0.856	-	0.942	-
Trifolium alpinum	0.606	-	0.69	-	0.661	-	0.655	-	0.651	-
Trifolium montanum	0.824	-	0.833	-	0.92	-	0.836	-	0.915	-
Trisetum flavescens	0.888	-	0.871	-	0.925	-	0.886	-	0.932	-
Vaccinium uliginosum subsp. *microphyllum*	0.841	-	0.798	-	0.86	-	0.811	-	0.841	-
Veronica allionii	0.708	-	0.619	-	0.689	-	0.665	-	0.697	-
Alchemilla xanthochlora aggr	0.629	0.601	0.612	0.603	0.608	0.588	0.59	0.636	0.617	0.631
Anthoxanthum odoratum aggr	0.591	0.704	0.624	0.641	0.628	0.671	0.618	0.638	0.629	0.68
Anthyllis vulneraria sl.	0.681	0.75	0.624	0.66	0.666	0.727	0.616	0.65	0.662	0.75
Arnica montana	0.828	0.617	0.802	0.66	0.83	0.659	0.758	0.71	0.822	0.645
Bartsia alpina	0.699	0.629	0.657	0.705	0.769	0.658	0.641	0.643	0.71	0.645
Campanula scheuchzeri	0.641	0.643	0.685	0.709	0.685	0.681	0.698	0.651	0.661	0.629
Carex sempervirens	0.628	0.76	0.608	0.648	0.598	0.755	0.605	0.655	0.596	0.709
Carlina acaulis subsp. *caulescens*	0.81	0.723	0.786	0.744	0.823	0.771	0.791	0.691	0.853	0.783
Cirsium spinosissimum	0.681	0.671	0.629	0.681	0.7	0.71	0.688	0.686	0.742	0.735
Dryas octopetala	0.769	0.694	0.812	0.71	0.847	0.733	0.816	0.685	0.881	0.697
Festuca rubra aggr.	0.681	0.658	0.706	0.76	0.711	0.79	0.709	0.716	0.693	0.706
Festuca violacea aggr.	0.609	0.634	0.608	0.608	0.586	0.599	0.595	0.63	0.62	0.642
Gentiana acaulis	0.729	0.72	0.709	0.68	0.758	0.72	0.645	0.693	0.737	0.738
Geum montanum	0.645	0.603	0.593	0.709	0.607	0.68	0.579	0.758	0.638	0.687
Homogyne alpina	0.896	0.615	0.799	0.625	0.878	0.656	0.81	0.605	0.901	0.623

Leontodon helveticus	0.59	0.677	0.666	0.746	0.642	0.772	0.663	0.71	0.615	0.715
Leontodon hispidus sl.	0.802	0.659	0.8	0.645	0.818	0.699	0.735	0.61	0.859	0.665
Lotus corniculatus aggr.	0.862	0.616	0.71	0.608	0.859	0.608	0.713	0.601	0.901	0.61
Myosotis alpestris	0.672	0.729	0.713	0.639	0.735	0.664	0.735	0.608	0.753	0.693
Nardus stricta	0.654	0.613	0.624	0.659	0.644	0.655	0.625	0.667	0.641	0.647
Phleum rhaeticum	0.68	0.683	0.75	0.576	0.724	0.682	0.718	0.653	0.692	0.701
Phyteuma orbiculare	0.631	0.66	0.614	0.62	0.603	0.626	0.625	0.614	0.578	0.638
Plantago alpina	0.619	0.618	0.621	0.621	0.619	0.631	0.671	0.59	0.635	0.588
Poa alpina	0.788	0.647	0.619	0.633	0.795	0.655	0.625	0.627	0.764	0.64
Polygonum viviparum	0.718	0.652	0.653	0.685	0.698	0.691	0.722	0.615	0.743	0.655
Potentilla aurea	0.625	0.612	0.669	0.746	0.659	0.75	0.571	0.745	0.596	0.725
Ranunculus acris sl.	0.664	0.68	0.748	0.665	0.748	0.662	0.803	0.731	0.799	0.681
Ranunculus montanus aggr.	0.684	0.599	0.745	0.652	0.744	0.642	0.727	0.714	0.781	0.677
Salix herbacea	0.741	0.655	0.781	0.686	0.818	0.639	0.791	0.62	0.811	0.669
Sesleria caerulea	0.666	0.655	0.752	0.705	0.737	0.718	0.797	0.671	0.783	0.713
Thesium alpinum	0.71	0.66	0.793	0.781	0.791	0.747	0.84	0.718	0.788	0.678
Thymus praecox subsp. *polytrichus*	0.771	0.649	0.694	0.748	0.803	0.717	0.655	0.757	0.756	0.649
Trifolium pratense sl.	0.759	0.592	0.66	0.75	0.72	0.731	0.67	0.697	0.732	0.678
Trifolium repens sstr.	0.651	0.747	0.609	0.691	0.611	0.746	0.639	0.786	0.673	0.749
Trifolium thalii	0.623	0.606	0.66	0.612	0.612	0.607	0.635	0.606	0.634	0.616
Vaccinium myrtillus	0.882	0.647	0.801	0.671	0.858	0.623	0.779	0.643	0.848	0.659
Viola calcarata	0.627	0.68	0.613	0.614	0.624	0.616	0.624	0.737	0.622	0.628
Agrostis capillaris	-	0.66	-	0.771	-	0.774	-	0.793	-	0.852
Agrostis rupestris	-	0.685	-	0.762	-	0.721	-	0.598	-	0.666
Alchemilla conjuncta aggr.	-	0.599	-	0.684	-	0.697	-	0.669	-	0.629
Alchemilla glabra aggr.	-	0.671	-	0.736	-	0.705	-	0.619	-	0.66
Alchemilla vulgaris aggr.	-	0.74	-	0.634	-	0.65	-	0.655	-	0.674
Androsace chamaejasme	-	0.658	-	0.602	-	0.643	-	0.61	-	0.646
Aposeris foetida	-	0.788	-	0.714	-	0.818	-	0.692	-	0.838
Aster bellidiastrum	-	0.705	-	0.646	-	0.741	-	0.657	-	0.758
Campanula barbata	-	0.703	-	0.789	-	0.745	-	0.787	-	0.72
Carex ornithopoda	-	0.707	-	0.638	-	0.68	-	0.612	-	0.677
Cerastium fontanum sl.	-	0.682	-	0.684	-	0.706	-	0.683	-	0.685
Crepis aurea	-	0.634	-	0.716	-	0.639	-	0.636	-	0.597
Crocus albiflorus	-	0.744	-	0.733	-	0.769	-	0.727	-	0.781
Deschampsia cespitosa	-	0.683	-	0.715	-	0.726	-	0.773	-	0.754
Euphrasia minima	-	0.585	-	0.66	-	0.624	-	0.6	-	0.606
Festuca quadriflora	-	0.634	-	0.767	-	0.737	-	0.679	-	0.647
Galium anisophyllon	-	0.767	-	0.609	-	0.753	-	0.713	-	0.771
Gentiana campestris sstr.	-	0.705	-	0.597	-	0.665	-	0.65	-	0.673
Gentiana purpurea	-	0.62	-	0.81	-	0.797	-	0.788	-	0.746
Gentiana verna	-	0.682	-	0.681	-	0.663	-	0.674	-	0.646
Helianthemum nummularium sl.	-	0.631	-	0.631	-	0.627	-	0.638	-	0.624
Helictotrichon versicolor	-	0.627	-	0.607	-	0.615	-	0.597	-	0.605
Hieracium lactucella	-	0.648	-	0.755	-	0.761	-	0.771	-	0.748

Leucanthemum vulgare aggr.	-	0.864	-	0.756	-	0.888	-	0.707	-	0.911
Ligusticum mutellina	-	0.624	-	0.677	-	0.671	-	0.741	-	0.698
Loiseleuria procumbens	-	0.66	-	0.639	-	0.601	-	0.635	-	0.624
Luzula alpinopilosa	-	0.671	-	0.69	-	0.681	-	0.711	-	0.688
Luzula multiflora	-	0.715	-	0.582	-	0.643	-	0.608	-	0.684
Pedicularis verticillata	-	0.682	-	0.657	-	0.693	-	0.627	-	0.681
Plantago atrata sstr.	-	0.6	-	0.614	-	0.607	-	0.605	-	0.593
Polygala alpestris	-	0.633	-	0.643	-	0.637	-	0.702	-	0.615
Potentilla crantzii	-	0.639	-	0.67	-	0.635	-	0.657	-	0.625
Prunella vulgaris	-	0.683	-	0.622	-	0.661	-	0.63	-	0.634
Salix retusa	-	0.68	-	0.688	-	0.764	-	0.661	-	0.748
Scabiosa lucida	-	0.647	-	0.678	-	0.727	-	0.607	-	0.633
Soldanella alpina	-	0.642	-	0.717	-	0.717	-	0.683	-	0.677
Taraxacum officinale aggr.	-	0.757	-	0.627	-	0.685	-	0.761	-	0.681
Trifolium badium	-	0.689	-	0.696	-	0.666	-	0.695	-	0.66
Trollius europaeus	-	0.667	-	0.812	-	0.8	-	0.715	-	0.75
Vaccinium gaultherioides	-	0.633	-	0.648	-	0.641	-	0.624	-	0.647
Vaccinium vitis-idaea	-	0.705	-	0.666	-	0.674	-	0.644	-	0.723

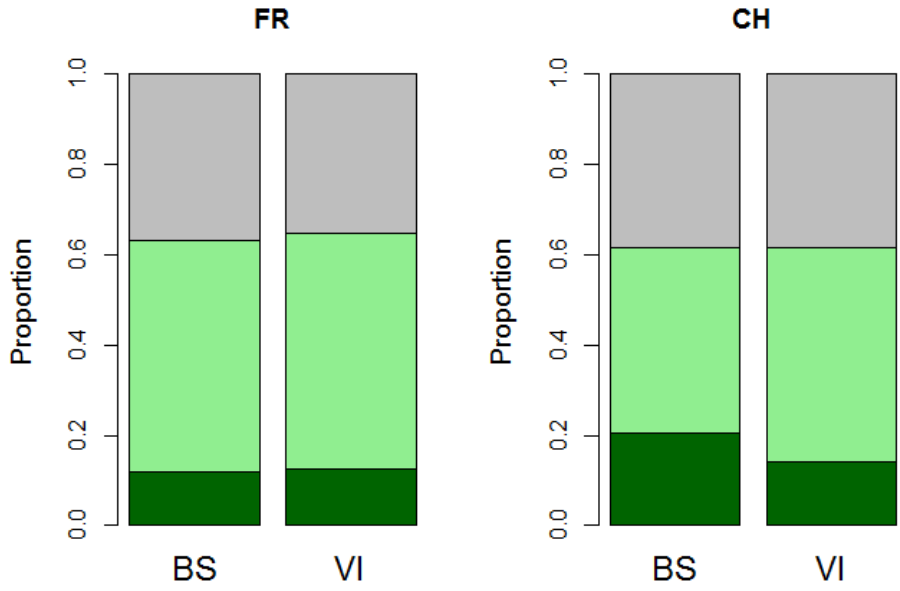

ESM2 Fig 3: Proportions of species distribution models for which accuracy was improved by 10% (dark green areas) or between 0 and 10% (light green areas) or was declined (gray areas) when adding the AIS-predictors to topographic based models. FR for the French site and CH for the Swiss site. BS indicates reflectance records in spectral bands as predictors and VI indicates vegetation indices as predictors. See ESM2 Table 1 for identity of the species that showed best model improvement.

Weak or no improvement of species distribution models, when including AIS-predictors, suggests that the ecological information represented by AIS-data was redundant to already included topography indicators. Increasing the dimensionality of the set of predictors without additional informational content may flaw the fitted statistical relationships and ultimately decrease model accuracy as we observed for many species at both sites.

4) The effect of species abundance patterns on the prediction accuracy of remote sensing–based species distribution models.

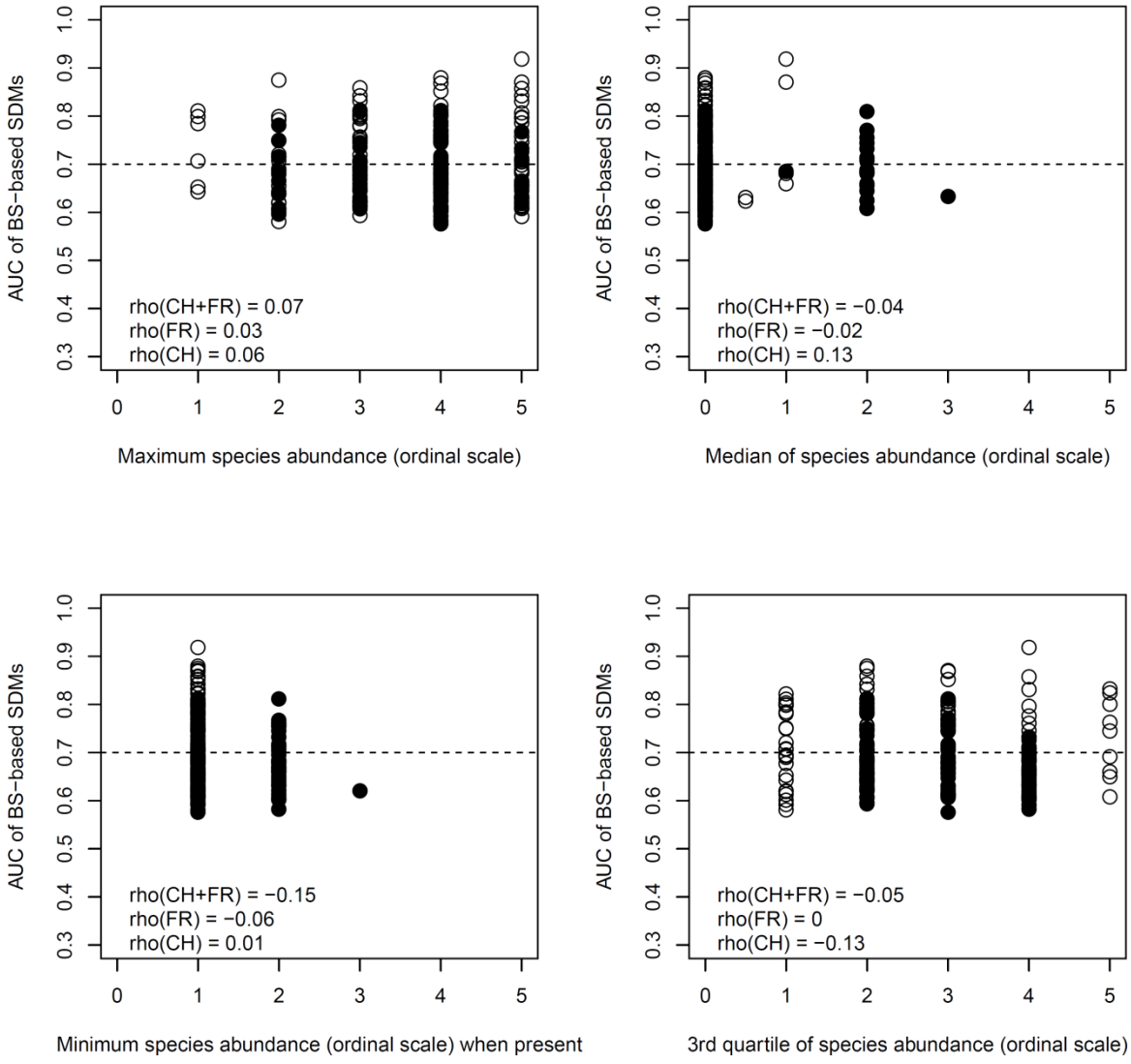

ESM2 Fig 4: Relationships between four predictors of species abundance patterns and the accuracy of species distribution models based on the reflectance records in spectral bands (BS). White points for species from the French site (FR) and black points for species from the Swiss site (CH).

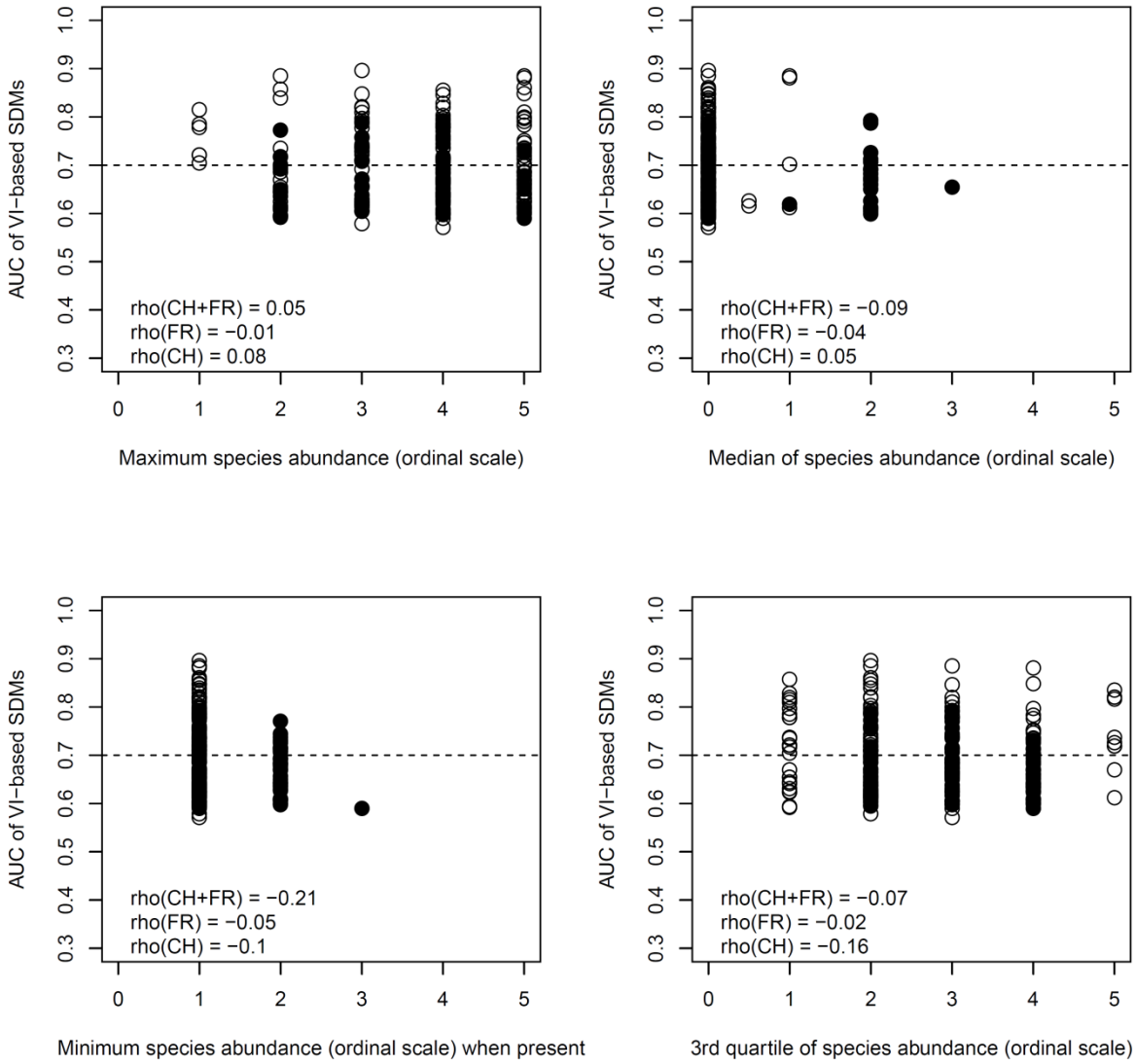

ESM2 Fig 5: Relationships between four predictors of species abundance patterns and the accuracy of species distribution models based on the vegetation indices. White points for species from the French site (FR) and black points for species from the Swiss site (CH).

5) Testing the phylogenetic and functional dependency of model features between the species.

We implemented a similar procedure as for the test of phylogenetic signal of species traits, except were considered the AUC values and AIS-predictor importance as traits and we sought for both phylogenetic and functional signals. Specifically, we implemented two complementary analyses following recommendations of Hardy and Pavoine 2012 [1]. In the first, we computed a global Mantel test contrasting dissimilarity of species distribution models (Euclidean distance between AUC values or AIS-variable importance) and phylogenetic or functional dissimilarity between the species. The randomisation procedure consisted of random reallocation of AUC values or variable importance between the species (999 permutations). In the second, we computed distograms where species model dissimilarities (again as Euclidean distance between AUC values or AIS-variable importance) are plotted against classes of phylogenetic or functional distance between the species. This indicates how species models differ for functionally/phylogenetically closely related species and for dissimilar species.

Phylogenic information for the French site was extracted from the complete phylogeny for the Alpine flora at the genus level published in Thuiller et al. 2014 [2]. Finally, we randomly resolved terminal polytomies by applying a birth-death (Yule) bifurcation process within each genus [3]. Phylogenetic information for the Swiss site was extracted from the phylogeny for the 231 most frequent species of the Western Swiss Alps of the Canton of Vaud (a 700 km² region surrounding the Swiss site Anzeindaz). This phylogeny is based on DNA sequences extracted from collected vegetal material and built by alignment of chloroplastic DNA sequences (*rbcl* and *matK*) with GTR + gamma models of evolution under a Bayesian inference framework. Details are available in Ndiribe et al. 2013 [4].

All the species of the French site (i.e. 119) were included in phylogenetic tests while 69 species of the Swiss site (on 78) could be accounted for.

The phylogenetic distance between the species was quantified using the Abouheif proximity measure for Mantel tests and the square-root of patristic distance for distograms [1].

Traits information included morphological and physiological traits that are acknowledged to indicate plant fitness, community dynamics and ecosystem processes. Some of them are also recognized to be related to the reflectance pattern of vegetation stands [5,6]. We considered: 1) specific leaf area (SLA; $m^2.kg^{-1}$), 2) leaf dry matter content (LDMC, $mg.g^{-1}$), 3) vegetation

height (mm), 4) plant growth form discriminating species as graminoid, forb, legume or shrub, 5) Leaf distribution along the stem discriminating species with leaves growing regularly along the stem, rosette or tufted species and semi rosette species, and 6) branching, a binary trait describing species ability to fill lateral space. SLA, LDMC and vegetation height were measured for most species in the field within each of the two sites (89 out 119 for FR and 71 out of 78 for CH). Leaf distribution, growth form, and branching were retrieved from the LEDA database [7]. Since trait data covered continuous and categorical variables, the functional dissimilarity between species was quantified using the Gower distance metric [8] for both Mantel tests and distogram computation.

Tests for phylogenetic and functional dependency of the importance of AIS-variables considered only the species that showed distribution models with fair to good prediction accuracy (i.e. AUC > 0.7) in order to exclude spurious estimates of variable importance from inaccurate models. This led to analyses with reduced list of species as follows:

Number of species included in the analyses	FR		CH	
	Phylogenetic (119/119sp)	Functional (89/119sp)	Phylogenetic (69/78sp)	Functional (71/78sp)
Reflectance in spectral bands	64	47	25	25
Vegetation indices	68	50	19	20

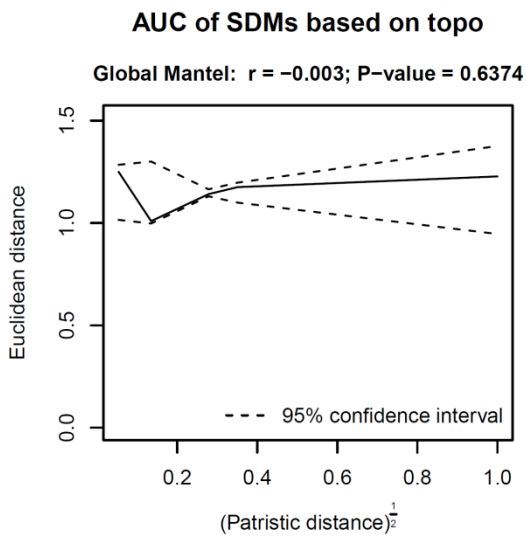

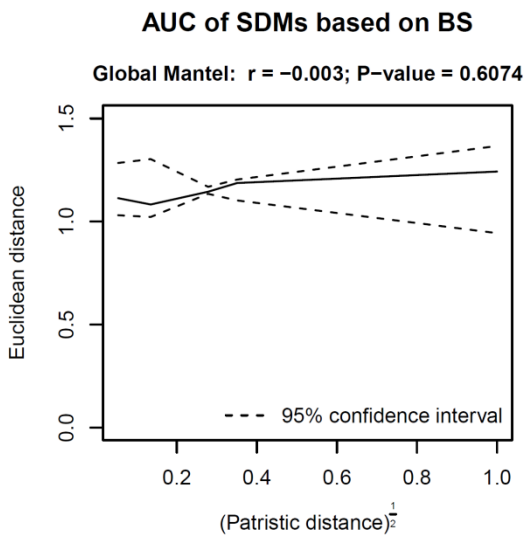

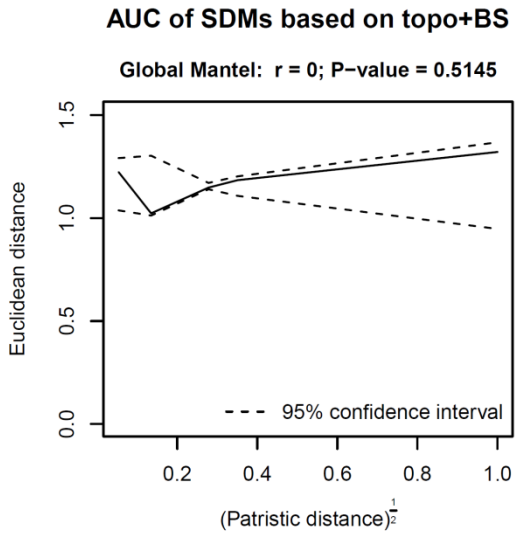

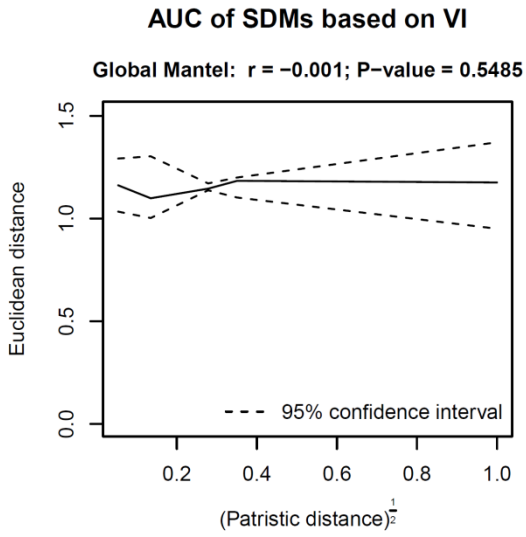

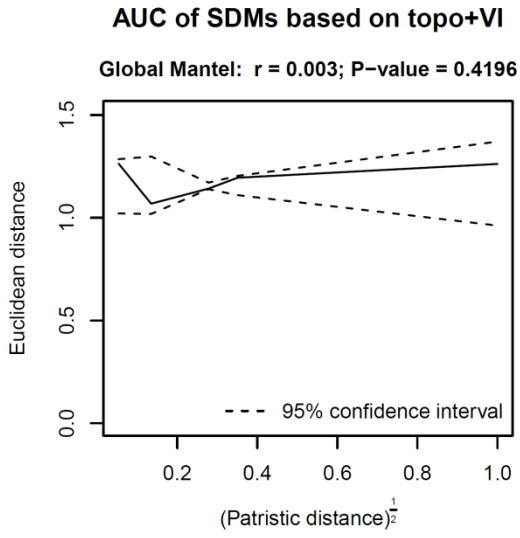

ESM2 Fig 6: **Phylogenetic dependency of model accuracy** (AUC: the area under the curve of a receiver-operating characteristic plot) between the species for the **French site (FR)**. The x-axis represents the phylogenetic distance between the species and the y-axis differences in AUC. Topo indicates models based on topographic predictors only, BS models based on reflectance recorded in the spectral bands. VI indicates models based on vegetation indices only. Topo+BS and Topo+VI indicate respectively models based on topographic predictors and reflectance records in spectral bands or vegetation indices as predictors. Confidence intervals were computed with random re-allocation of AUC values between the species (9999 permutations)

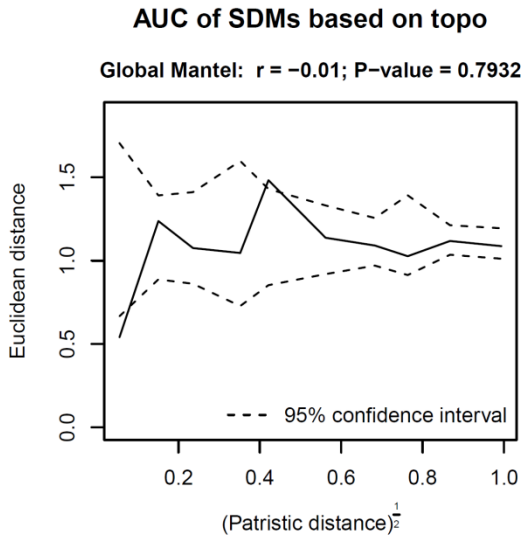

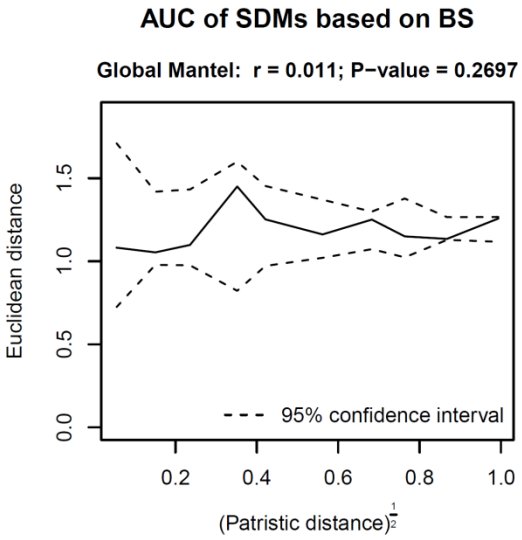

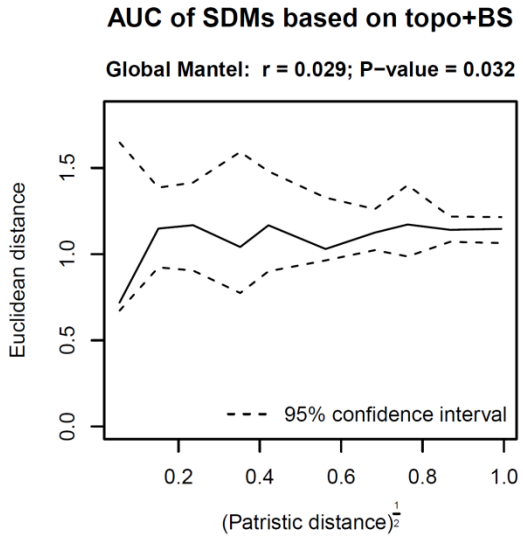

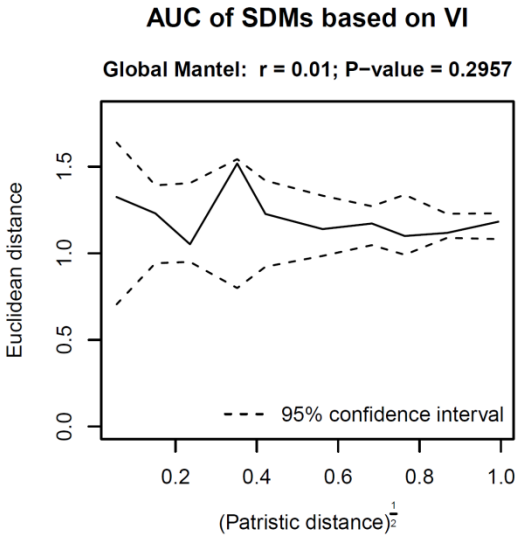

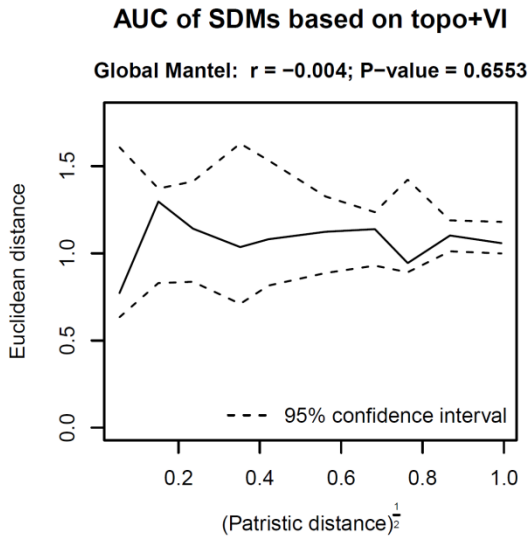

ESM2 Fig 7: **Phylogenetic dependency of model accuracy** (AUC: the area under the curve of a receiver-operating characteristic plot) between the species for the **Swiss site (CH)**. The x-axis represents the phylogenetic distance between the species and the y-axis differences in AUC. Topo indicates models based on topographic predictors only, BS models based on reflectance recorded in the spectral bands. VI indicates models based on vegetation indices only. Topo+BS and Topo+VI indicate respectively models based on topographic predictors and reflectance records in spectral bands or vegetation indices as predictors. Confidence intervals were computed with random re-allocation of AUC values between the species (9999 permutations)

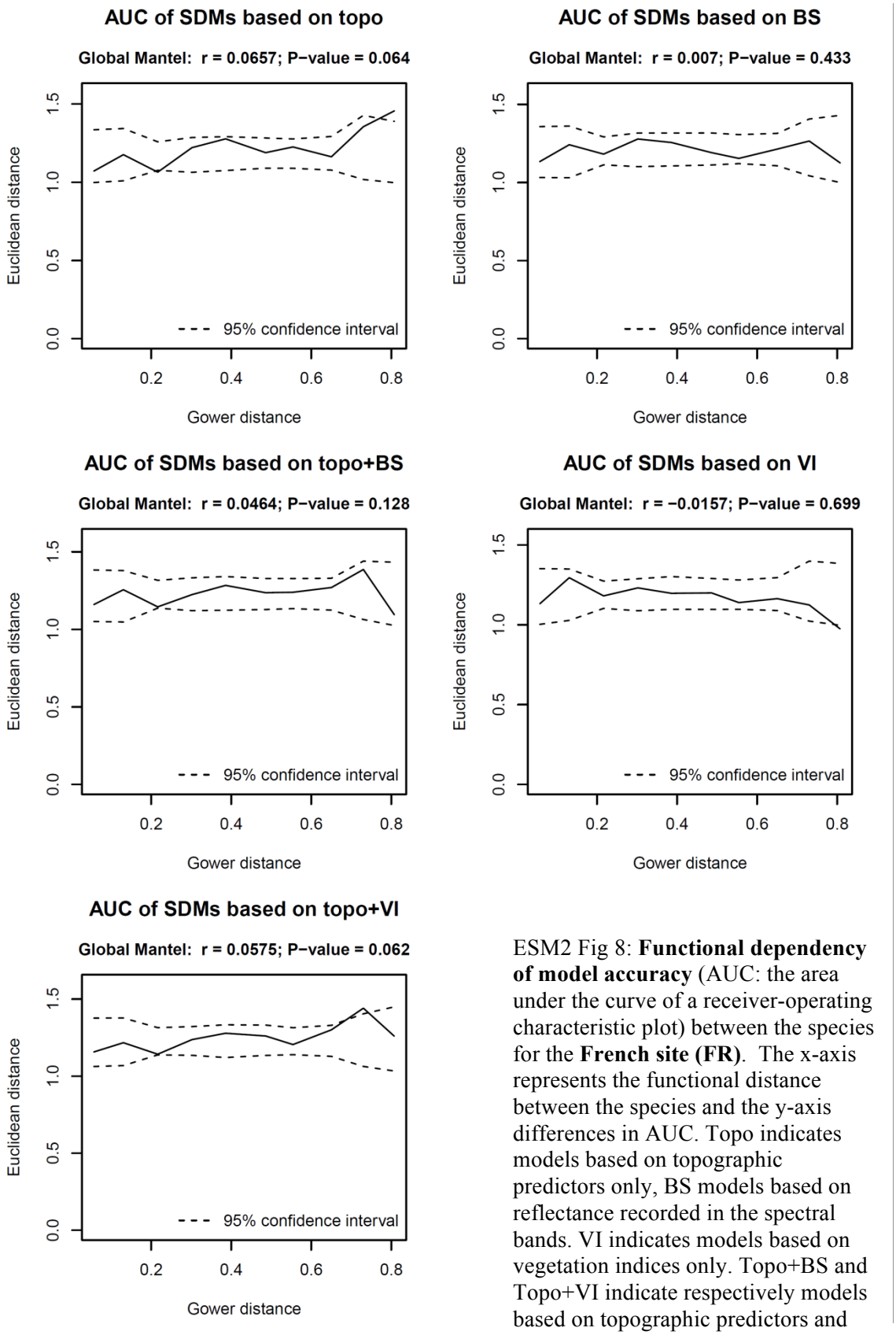

ESM2 Fig 8: **Functional dependency of model accuracy** (AUC: the area under the curve of a receiver-operating characteristic plot) between the species for the **French site (FR)**. The x-axis represents the functional distance between the species and the y-axis differences in AUC. Topo indicates models based on topographic predictors only, BS models based on reflectance recorded in the spectral bands. VI indicates models based on vegetation indices only. Topo+BS and Topo+VI indicate respectively models based on topographic predictors and reflectance records in spectral bands or vegetation indices as predictors. Confidence intervals were computed with random re-allocation of AUC values between the species (9999 permutations)

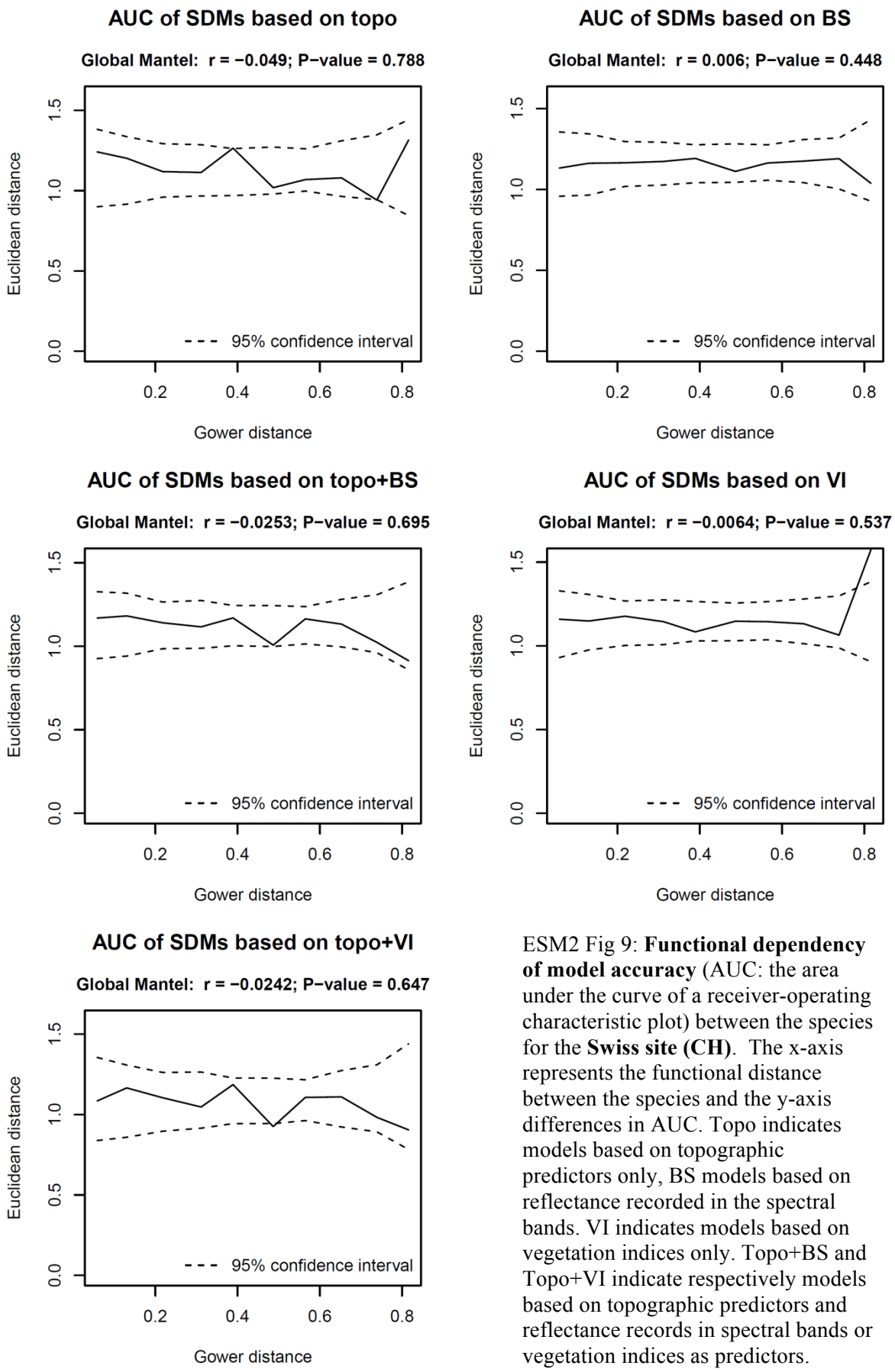

ESM2 Fig 9: **Functional dependency of model accuracy** (AUC: the area under the curve of a receiver-operating characteristic plot) between the species for the **Swiss site (CH)**. The x-axis represents the functional distance between the species and the y-axis differences in AUC. Topo indicates models based on topographic predictors only, BS models based on reflectance recorded in the spectral bands. VI indicates models based on vegetation indices only. Topo+BS and Topo+VI indicate respectively models based on topographic predictors and reflectance records in spectral bands or vegetation indices as predictors. Confidence intervals were computed with random re-allocation of AUC values between the species (9999 permutations)

581
582

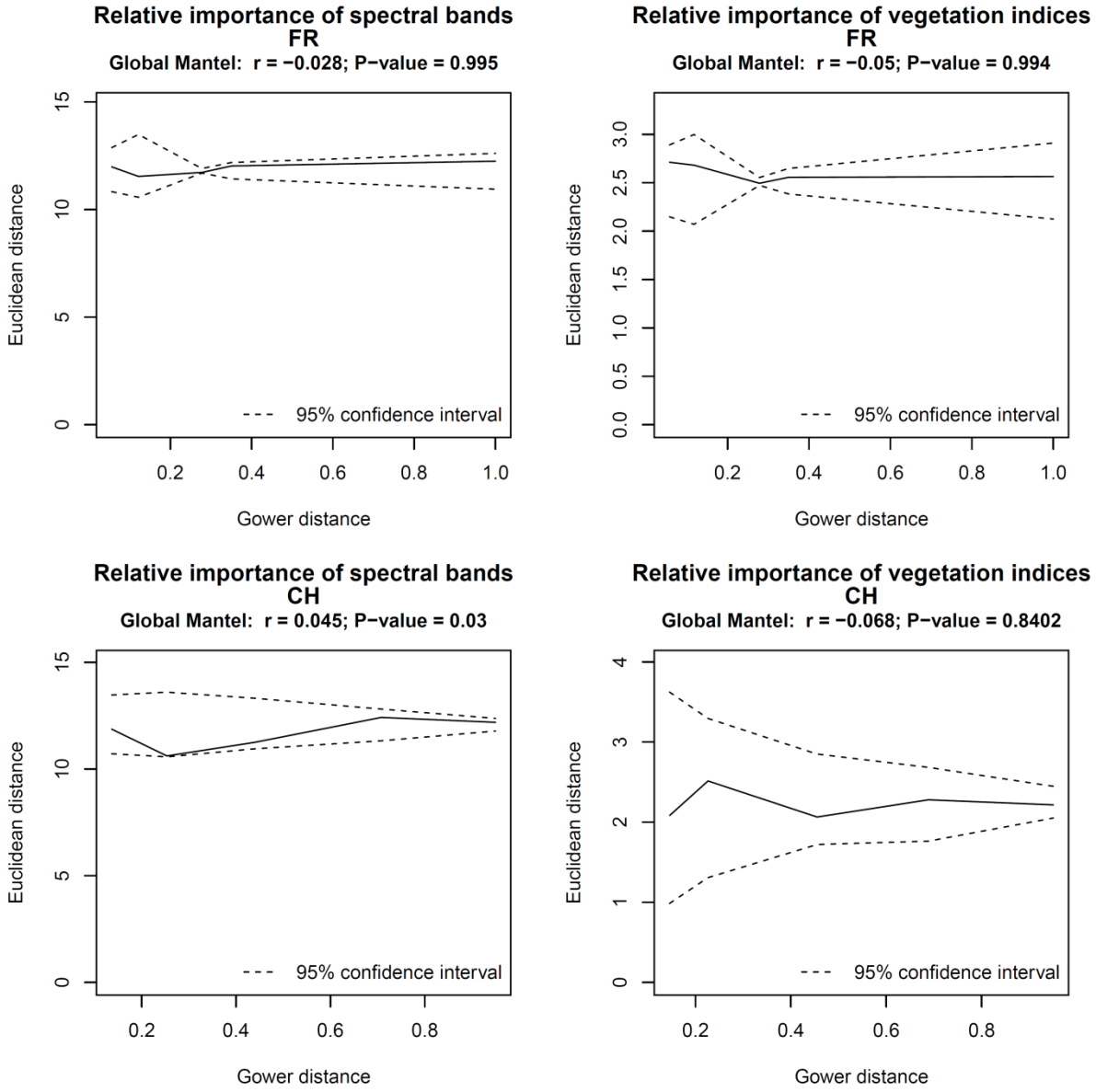

583
584
585

ESM2 Fig 10: **Phylogenetic dependency of relative importance of AIS-predictors** between the species for both the French site (FR) and the Swiss site (CH). The x-axis represents the phylogenetic distance between the species and the y-axis differences in RS-predictors (either reflectance recorded in the spectral bands or vegetation indices). Only species with distribution models showing fair to good prediction accuracy (AUC>0.7) were considered. Confidence intervals were computed with random re-allocation of predictor importance between the species (9999 permutations)

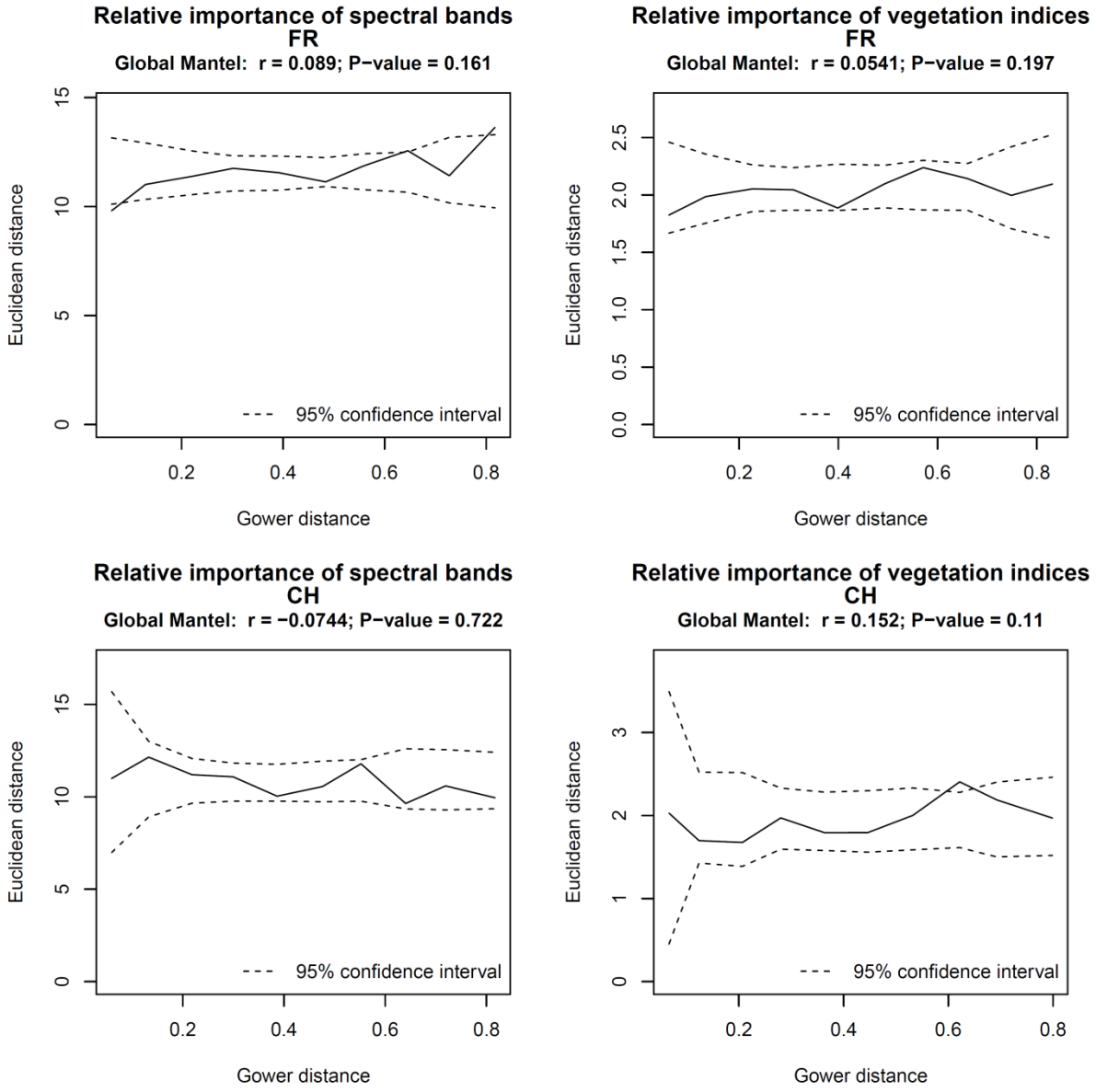

ESM2 Fig 11: **Functional dependency of relative importance of RS-predictors** between the species for both the French site (FR) and the Swiss site (CH). The x-axis represents the functional distance between the species and the y-axis differences in AIS-predictors (either reflectance recorded in the spectral bands or vegetation indices). Only species with distribution models showing fair to good prediction accuracy (AUC>0.7) were considered. Confidence intervals were computed with random re-allocation of predictor importance between the species (9999 permutations)

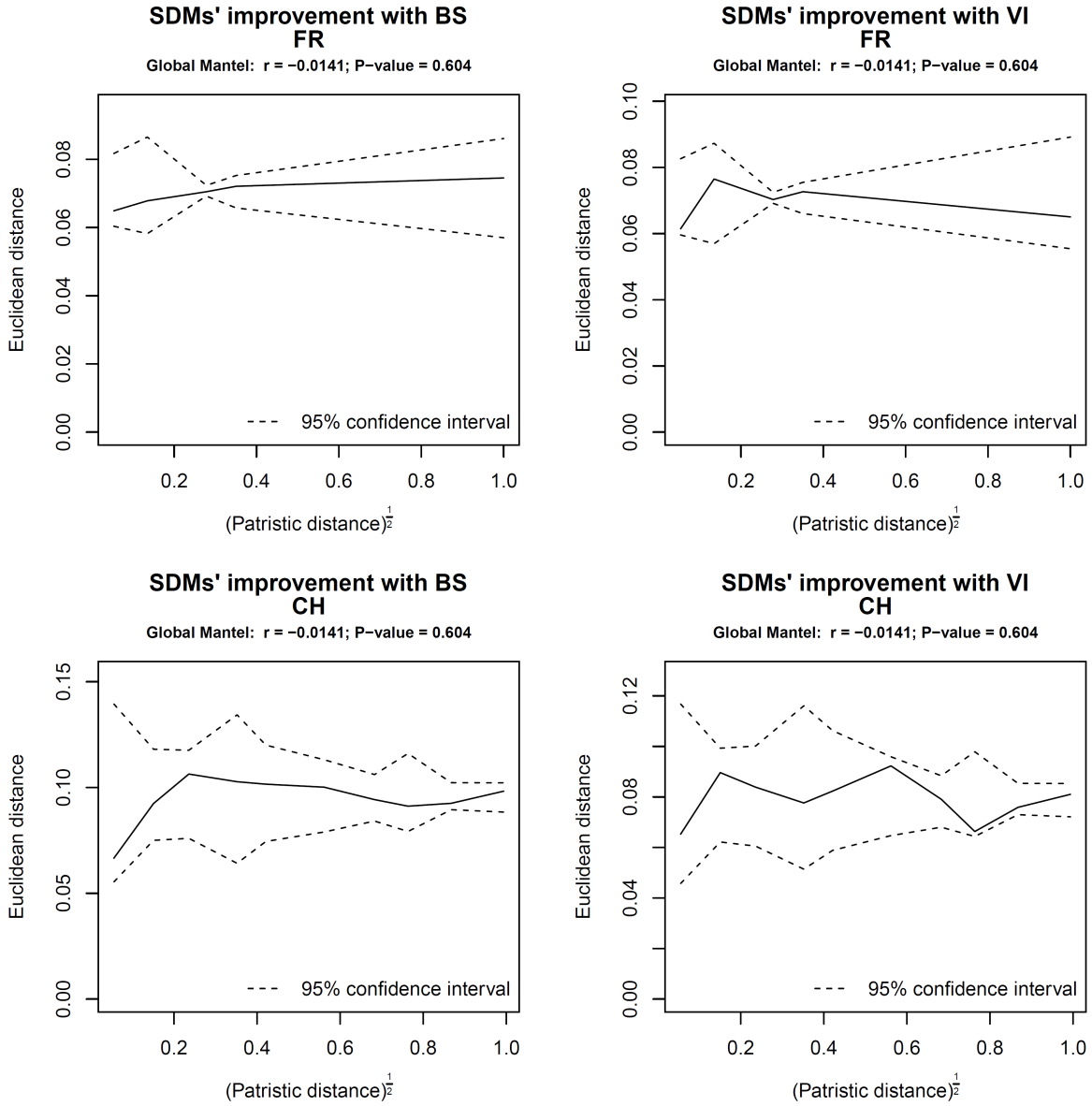

ESM2 Fig 12: **Phylogenetic dependency of model improvement among species with addition of AIS-predictors** for the French site (FR) and the Swiss site (CH). The x-axis represents the phylogenetic distance between the species and the y-axis differences in model improvement when adding AIS-predictors (either reflectance recorded in the spectral bands (BS) or vegetation indices (VI)) to topographic predictors. Confidence intervals were computed with random re-allocation of AUC values between the species (9999 permutations)

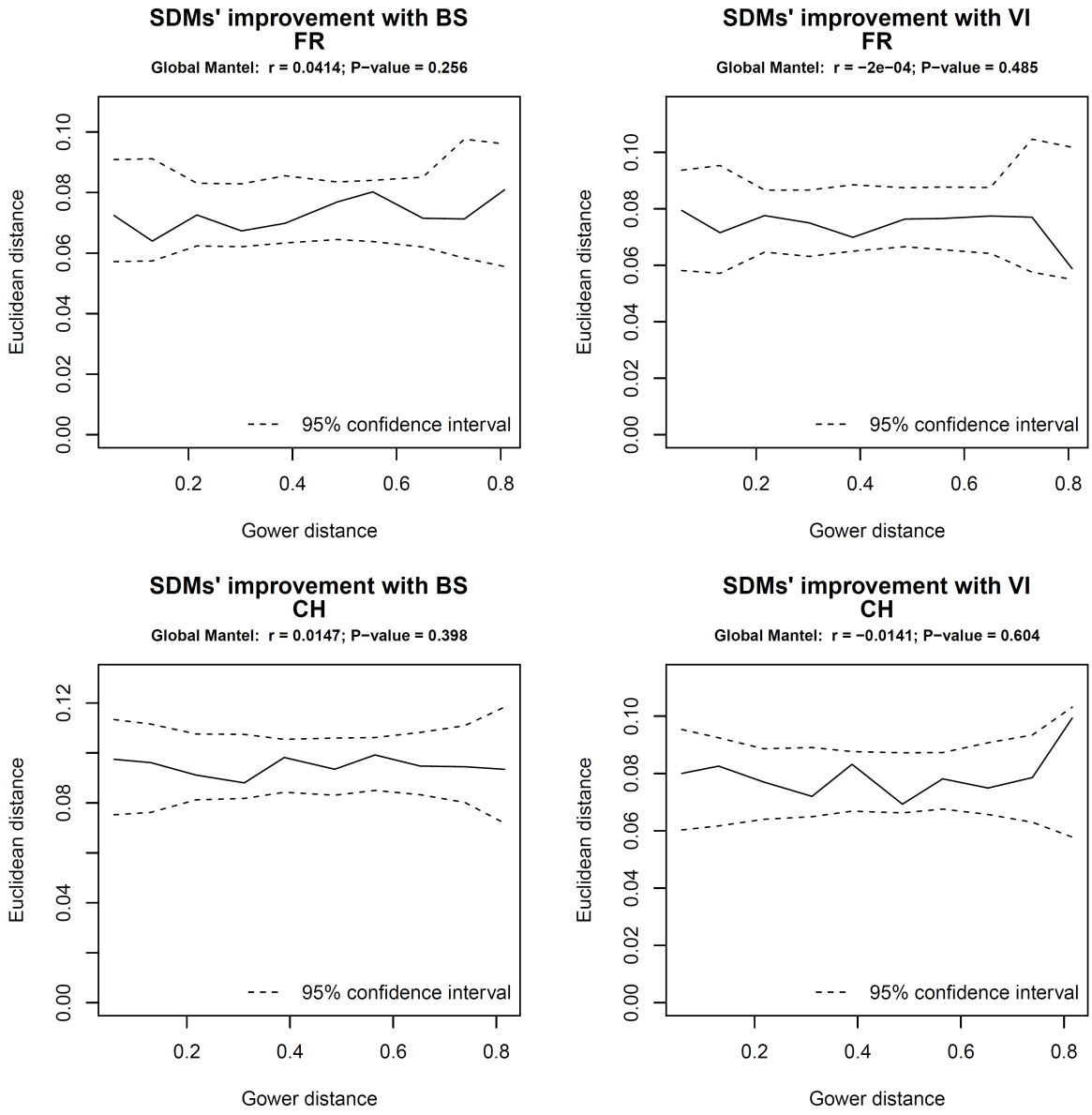

600

601

ESM2 Fig 13: **Functional dependency of model improvement among species with addition of AIS-predictors** for the French site (FR) and the Swiss site (CH). The x-axis represents the functional distance between the species and the y-axis differences in model improvement when adding AIS-predictors (either reflectance recorded in the spectral bands (BS) or vegetation indices (VI)) to topographic predictors. Confidence intervals were computed with random re-allocation of AUC values between the species (9999 permutations)

References

1. Hardy, O. J. & Pavoine, S. 2012 Assessing phylogenetic signal with measurement error: a comparison of Mantel tests, Blomberg et al.'s K, and phylogenetic distograms. *Evolution* **66**, 2614–21. (doi:10.1111/j.1558-5646.2012.01623.x)

2. Thuiller, W. et al. 2014 Are different facets of plant diversity well protected against climate and land cover changes? A test study in the French Alps. *Ecography (Cop.).* , Early view. (doi:10.1111/ecog.00670)

3. Roquet, C., Thuiller, W. & Lavergne, S. 2013 Building megaphylogenies for macroecology: taking up the challenge. *Ecography (Cop.).* **36**, 13–26. (doi:10.1111/j.1600-0587.2012.07773.x)

4. Ndiribe, C., Pellissier, L., Antonelli, S., Dubuis, A., Pottier, J., Vittoz, P., Guisan, A. & Salamin, N. 2013 Phylogenetic plant community structure along elevation is lineage specific. *Ecol. Evol.* **3**, 4925–39. (doi:10.1002/ece3.868)

5. Ollinger, S. V 2011 Sources of variability in canopy reflectance and the convergent properties of plants. *New Phytol.* **189**, 375–94. (doi:10.1111/j.1469-8137.2010.03536.x)

6. Homolová, L., Malenovský, Z., Clevers, J. G. P. W., García-Santos, G. & Schaepman, M. E. 2013 Review of optical-based remote sensing for plant trait mapping. *Ecol. Complex.* **15**, 1–16. (doi:10.1016/j.ecocom.2013.06.003)

7. Kleyer, M. et al. 2008 The LEDA Traitbase: a database of life-history traits of the Northwest European flora. *J. Ecol.* **96**, 1266–1274. (doi:10.1111/j.1365-2745.2008.01430.x)

8. Gower, J. 1971 A general coefficient of similarity and some of its properties. *Biometrics* **27**, 857–871.

628 Airborne imaging spectroscopy (AIS) can provide remotely sensed estimates of physical and
629 bio-chemical quantitative properties of ecosystems. However, the value of these
630 characteristics for predicting diversity patterns has not been tested yet. We assess the added
631 value of such data for predicting plant distributions in French and Swiss alpine grasslands. We
632 fitted statistical models with high spectral and spatial resolution reflectance data and with four
633 optical indices sensitive to leaf chlorophyll content, leaf water content and leaf area index. We
634 found moderate added value of AIS-data for predicting alpine plant species distribution,
635 revealing issues of scale and AIS-data informational content.
636